Defining the signalling determinants of a posterior ventral spinal cord identity in human neuromesodermal progenitor derivatives

Matthew Wind[1,2,3], Antigoni Gogolou[1,2,3], Ichcha Manipur[4], Ilaria Granata[4], Larissa Butler[1], Peter W. Andrews[1], Ivana Barbaric[1], Ke Ning[3,5], Mario R. Guarracino[6], Marysia Placzek[2] and Anestis Tsakiridis[1,2,3,*]

ABSTRACT

The anteroposterior axial identity of motor neurons (MNs) determines their functionality and vulnerability to neurodegeneration. Thus, it is a crucial parameter in the design of strategies aiming to produce MNs from human pluripotent stem cells (hPSCs) for regenerative medicine/disease modelling applications. However, the *in vitro* generation of posterior MNs corresponding to the thoracic/ lumbosacral spinal cord has been challenging. Although the induction of cells resembling neuromesodermal progenitors (NMPs), the bona fide precursors of the spinal cord, offers a promising solution, the progressive specification of posterior MNs from these cells is not well defined. Here, we determine the signals guiding the transition of human NMP-like cells toward thoracic ventral spinal cord neurectoderm. We show that combined WNT-FGF activities drive a posterior dorsal pre-/early neural state, whereas suppression of TGFβ-BMP signalling pathways promotes a ventral identity and neural commitment. Based on these results, we define an optimised protocol for the generation of thoracic MNs that can efficiently integrate within the neural tube of chick embryos. We expect that our findings will facilitate the comparison of hPSC-derived spinal cord cells of distinct axial identities.

KEY WORDS: Neuromesodermal progenitors, Human pluripotent stem cells, *In vitro* differentiation, Motor neurons, Regional identity, Spinal cord

INTRODUCTION

The developing spinal cord generates a diverse range of cell types including motor neurons (MNs). These control all muscle movements in the body and are therefore of great clinical importance in neurodegenerative conditions such as amyotrophic lateral sclerosis (ALS), as well as traumatic spinal cord injuries that cause paralysis. An attractive platform for the *in vitro* modelling and treatment of these conditions involves the generation of MNs from human pluripotent stem cells (hPSCs) via directed differentiation or

[1]Centre for Stem Cell Biology, Department of Biomedical Science, The University of Sheffield, Sheffield S10 2TN, UK. [2]Department of Biomedical Science and Bateson Centre, University of Sheffield, Sheffield S10 2TN, UK. [3]Department of Neuroscience, Neuroscience Institute, University of Sheffield, Western Bank, Sheffield S10 2TN, UK. [4]Computational and Data Science Laboratory, High Performance Computing and Networking Institute, National Research Council of Italy, Napoli 80131, Italy. [5]Sheffield Institute for Translational Neuroscience, Department of Neuroscience, University of Sheffield, Sheffield S10 2HQ, UK. [6]University of Cassino and Southern Lazio, Cassino 03043, Italy.

*Author for correspondence (a.tsakiridis@sheffield.ac.uk)

A.G., 0000-0002-3581-2426; I.M., 0000-0001-5348-8378; I.G., 0000-0002-3450-4667; I.B., 0000-0003-3120-9563; K.N., 0000-0002-0771-1134; M.P., 0000-0002-4106-9229; A.T., 0000-0002-2184-2990

transcriptional programming approaches (Davis-Dusenbery et al., 2014). During embryonic development, MNs arise from ventrally located spinal cord progenitors and subsequently become organised into longitudinally arrayed columns and pools connected to various muscle targets (reviewed by Sagner and Briscoe, 2019). The induction of MN subtypes and their subsequent muscle target specificity is determined by their position along the anteroposterior (A-P) axis. The A-P position of MNs also appears to influence their vulnerability to ALS (Brockington et al., 2013; Gerardo-Nava et al., 2013; Kaplan et al., 2014). Thus, the *in vitro* production of spinal cord cells/MNs of defined A-P axial identities from hPSCs is an important factor to consider in the design of regenerative medicine therapies and the study of axial level-specific neuroprotective mechanisms.

The A-P patterning of spinal cord MNs is orchestrated primarily by the coordinated action of Hox gene family members (Dasen et al., 2008, 2003, 2005; Jung et al., 2010; Lacombe et al., 2013; Mendelsohn et al., 2017; Philippidou and Dasen, 2013). Hox genes are arranged as paralogous groups (PG) (1-13) across four distinct chromosomal clusters (A, B, C and D) and they are expressed along the post-cranial A-P axis in a strict spatiotemporal manner reflecting their 3′-5′ genomic order (reviewed by Philippidou and Dasen, 2013). Hindbrain/cervical spinal cord MNs innervating facial, neck/ shoulder and diaphragm muscles are marked by the expression of Hox PG(1-5) members. Posterior brachial/thoracic spinal cord MNs innervating the upper limbs, hypaxial muscles and sympathetic ganglia are characterised by Hox PG(6-9) expression. MNs at the lumbosacral axial levels controlling lower limb movements are defined by expression of Hox PG(10-13) members. The preservation of this expression pattern in the adult spinal cord suggests additional role(s) for Hox genes in controlling axial identity-dependent cell function in the spinal cord after birth (Nichterwitz et al., 2016; Sabourin et al., 2009; Zeisel et al., 2018).

To date, most protocols aiming to generate ventral spinal cord cells and MNs from hPSCs induce predominantly cells of a mixed hindbrain/cervical axial identity marked by expression of Hox PG(1-5) members but are inefficient in producing high numbers of more posterior, thoracic/lumbosacral Hox PG(6-13)-positive spinal cord cells. The advent of culture regimens (both adherent and three-dimensional) promoting the induction of neuromesodermal progenitor (NMP)-like cells *in vitro* has opened new promising avenues toward the *in vitro* generation of 'hard-to-make' posterior MNs (Cooper et al., 2020 preprint; Faustino Martins et al., 2020; Gouti et al., 2014; Kumamaru et al., 2018; Libby et al., 2020 preprint; Lippmann et al., 2015; Mouilleau et al., 2020 preprint; Rayon et al., 2020; Turner et al., 2014; Verrier et al., 2018). NMPs are the posteriorly located multipotent cell population that gives rise to both ventral spinal cord and paraxial mesoderm/somites in amniote embryos (Cambray and Wilson, 2007; Guillot et al., 2020 preprint; Mugele et al., 2018 preprint; Tzouanacou et al., 2009;

Wood et al., 2019 preprint; Wymeersch et al., 2016; reviewed by Henrique et al., 2015) and are marked by the co-expression of early neural and mesodermal genes such as *Sox2* and brachyury (*T*) (Olivera-Martinez et al., 2012; Tsakiridis et al., 2014; Wymeersch et al., 2016). However, the yields of posterior MN populations produced using NMP-based protocols have been either undefined or low, especially in the case of two-dimensional, adherent differentiation protocols (Estevez-Silva et al., 2018; Lippmann et al., 2015; Rayon et al., 2020; Verrier et al., 2018), which give rise to MNs exhibiting, predominantly, a brachial rather than thoracic/lumbosacral identity (Estevez-Silva et al., 2018; Rayon et al., 2020; Verrier et al., 2018). This suggests that thorough characterisation of the progressive lineage restriction events underlying the neural differentiation of human NMPs *in vitro* is required for the optimisation and refinement of current posterior MN differentiation protocols.

In vivo, the induction/maintenance of NMPs is directed by the WNT and FGF signalling pathways (Amin et al., 2016; Anderson et al., 2020; Boulet and Capecchi, 2012; Cunningham et al., 2015; Delfino-Machin et al., 2005; Diez del Corral et al., 2002, 2003; Garriock et al., 2015; Goto et al., 2017; Jurberg et al., 2014; Nordstrom et al., 2006; Olivera-Martinez and Storey, 2007; Takemoto et al., 2006; Wymeersch et al., 2016; Young et al., 2009), which also drive the production of NMPs from PSCs *in vitro* (Gouti et al., 2014; Lippmann et al., 2015; Turner et al., 2014). Downstream neural differentiation of embryonic NMPs relies on high levels of somite-derived retinoic acid (RA) signalling acting on FGF-dependent, NMP-derived pre-neural precursors (Diez del Corral et al., 2002, 2003), whereas high WNT and FGF activities drive paraxial mesoderm specification (Garriock et al., 2015; Goto et al., 2017; Takada et al., 1994; Takemoto et al., 2011). WNT signals also act on Cdx transcription factors to trigger the acquisition of a posterior axial identity in NMPs and their derivatives (Amin et al., 2016; Delfino-Machin et al., 2005; Metzis et al., 2018; Nordstrom et al., 2006; van den Akker et al., 2002; Wymeersch et al., 2019; Young et al., 2009); reviewed by Deschamps and Duboule, 2017; Deschamps and van Nes, 2005). Moreover, dorsoventral (D-V) patterning of NMP-derived neurectoderm is mediated by the antagonistic action of pro-dorsal WNT/BMP/TGFβ and pro-ventral sonic hedgehog (SHH) signals (reviewed by Placzek and Briscoe, 2018; Sagner and Briscoe, 2019).

Here, we examine in detail the signal combinations directing the stepwise induction of posterior and ventral identities during the differentiation of adherent hPSC-derived NMP-like cells. We show that sustained WNT and high FGF signalling activity is sufficient to drive the transition of TBXT$^+$ (the human homologue of brachyury)-SOX2$^+$ NMP-like cells toward a pre-neural/early neural state in the absence of exogenous RA supplementation, which promotes further commitment of pre-neural cells to a definitive neural fate. This transition is accompanied by upregulation of HOX genes, a hallmark of posterior axial identity acquisition. WNT and FGF signals also promote a default dorsal identity and we demonstrate that efficient ventralisation and further neural commitment of WNT-FGF-induced pre-neural/early neural progenitors requires active suppression of the pro-dorsal TGFβ and BMP signalling pathways in addition to SHH signalling stimulation. Based on these findings, we define an optimised protocol for the generation of ventral spinal cord progenitors and MNs of a thoracic axial and, in particular, preganglionic columnar identity, and show that the resulting cells can efficiently integrate and establish appropriate neuronal projections within the posterior neural tube of chick embryos following transplantation. We anticipate that our

findings will pave the way for the development of novel cell replacement strategies aiming to treat posterior spinal cord injuries and enable the mechanistic dissection of the effect of axial identity on MN vulnerability to ALS.

RESULTS
WNT and FGF induce a posterior pre-/early neural state from human NMPs

The role of WNT and FGF signalling in NMP ontogeny *in vitro* has been unclear. Previous studies showed that their combined stimulation drives the induction of NMP-like cells from PSCs in the short term (Denham et al., 2015; Frith et al., 2018; Gouti et al., 2014; Lippmann et al., 2015) as well as their differentiation toward both neurectoderm and paraxial mesoderm following longer treatment (Cooper et al., 2020 preprint; Diaz-Cuadros et al., 2020; Edri et al., 2019; Frith et al., 2018; Gouti et al., 2014; Mouilleau et al., 2020 preprint; Tsakiridis and Wilson, 2015). We thus sought to test whether different WNT/FGF levels drive distinct cell fate decisions in human NMP-like cells. TBXT$^+$SOX2$^+$ cultures were generated following a 3-day treatment of hPSCs with recombinant FGF2 (20 ng/ml) and the WNT agonist/GSK-3 inhibitor CHIR99021 (CHIR) (3 µM) as described previously (Frith et al., 2018; Frith and Tsakiridis, 2019). NMP-like cells were subsequently re-plated and cultured in the presence of different concentrations of FGF2 (20, 100, 40 ng/ml) and CHIR (3, 8 µM) for distinct periods (Fig. 1A-C). We found that high levels of CHIR (8 µM) and FGF2 (40 ng/ml) promoted predominantly the generation of presomitic/paraxial mesoderm cells, marked by upregulation of *TBXT*, *MSGN1* and *PAX3* over a 2-day period (days 3-5) (Fig. 1, Fig. S1A,B). In contrast, a longer 4-day exposure of re-plated NMP-like cells in the presence of the same WNT/FGF agonist amounts that promoted their initial induction (3 µM CHIR and 20 ng/ml FGF2) resulted in the progressive reduction of TBXT-expressing cells/TBXT protein levels, which was further enhanced when higher levels of FGF2 were employed (100 ng/ml) in combination with CHIR (Fig. 1B-D; Fig. S1C). These data indicate that distinct levels and durations of WNT and FGF stimulation trigger different cell fate decisions in hPSC-derived NMP-like cells: high WNT activity combined with FGF signalling favours the generation of paraxial mesoderm, whereas lower WNT and high FGF levels drive the gradual extinction of TBXT$^+$ progenitors.

We next tested whether the dramatic TBXT reduction in day (D) 7 CHIR (3 µM) and FGF2 (100 ng/ml)-treated cultures is a consequence of their transition toward a neural fate. Indeed, we found that these cultures consisted predominantly of SOX2$^+$ (~90% of total) cells, most of which expressed CDX2 and HOXC9 (Fig. 2A-C). Transcriptome profiling following RNA sequencing confirmed that, with the exception of a few transcripts (*FBN2*, *CADM2*, *MEOX1*) that also mark neural crest/neural crest derivatives (Ansari et al., 2014; Candia et al., 1992; Diaz-Cuadros et al., 2020; Frith et al., 2018; Lumb et al., 2017; Shimada et al., 2012), paraxial mesoderm/somite/NMP markers (e.g. *TBXT*, *TBX6*, *MIXL1*, *EVX1*, *MSGN1*) were significantly downregulated (≥2-fold, FDR ≤0.05) or extinct in D7 cultures compared with D3 NMP-like cells (Fig. 2D, Fig. S2A, Table S1). However, the expression of NMP-associated genes linked to a subsequent pre-neural/early spinal cord identity (*NKX1-2*, *CDX1/2*) remained at high levels (Fig. 2D) and transcripts associated with neural lineage specification (e.g. *NEUROG2*, *ASXL3*, *POU3F2*, *IRX3*, *ONECUT2*) (Bosse et al., 1997; Delfino-Machin et al., 2005; Lichtig et al., 2020; Nordstrom et al., 2006; Sagner et al., 2018,
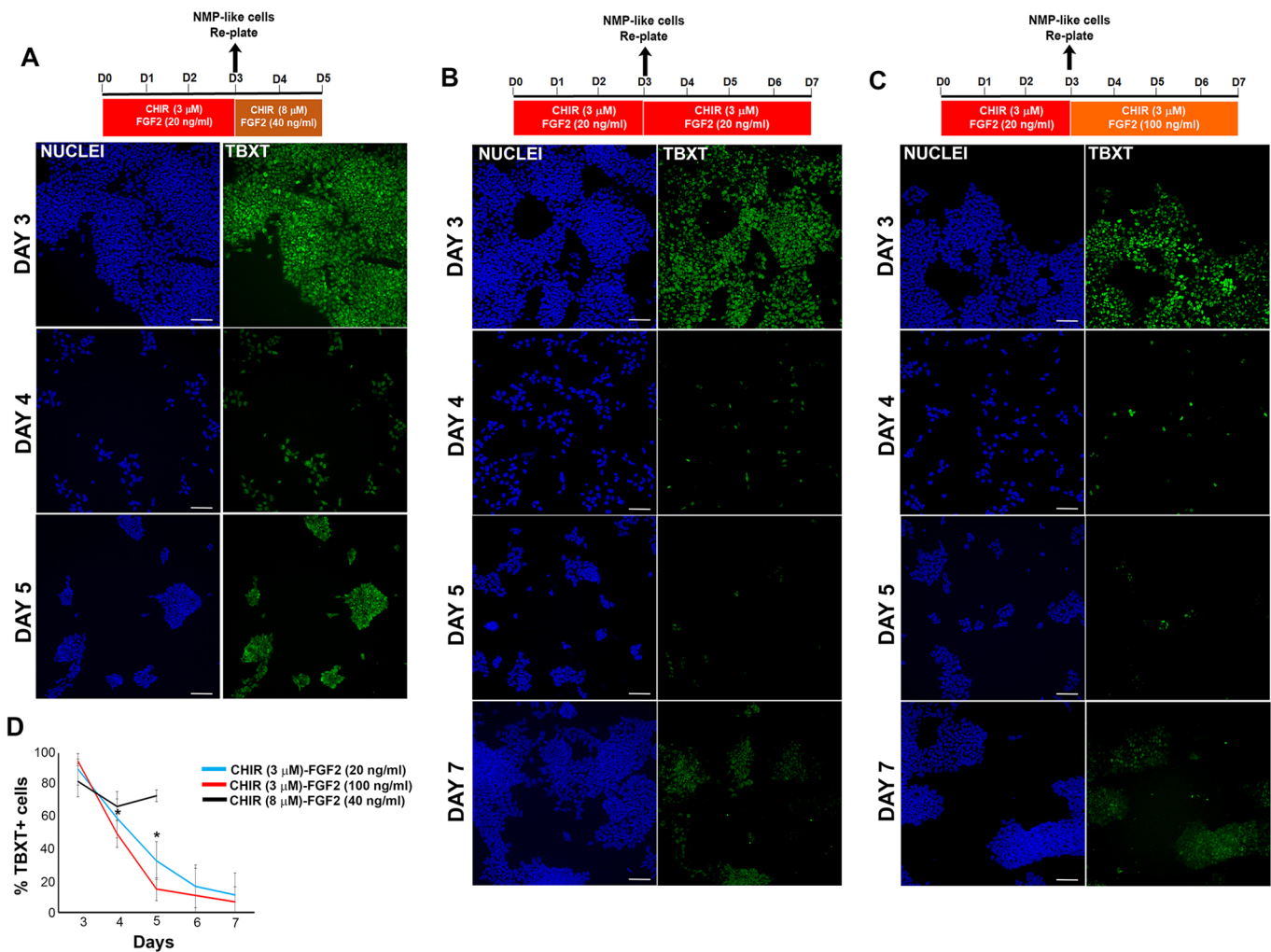
Fig. 1. Effect of distinct levels of WNT and FGF on NMP-like cells. (A-C) Time-course immunofluorescence analysis of the expression of TBXT protein in NMP-like cells (day 3; D3) and their differentiating derivatives following dissociation, re-plating and culture using the combinations of WNT and FGF agonists indicated in the schematics above. Scale bars: 100 µm. (D) Quantification of the percentage of TBXT$^+$ cells at different time points during treatment of NMP-like cells with the indicated combinations of WNT and FGF agonists. The data in the graph were obtained after scoring 10-25 random fields per experiment (four biological replicates for the experiments employing 3 µM CHIR, two biological replicates for the experiments employing 8 µM CHIR). Error bars represent s.d. *$P<0.05$ (paired t-test; comparison between CHIR 3 µM-FGF 20 ng/ml versus CHIR 3 µM-FGF2 100 ng/ml).

2020 preprint; Sommer et al., 1996) were significantly upregulated (≥2-fold, FDR ≤0.05) relative to D3 NMP-like cells (Fig. 2E, Fig. S2B, Table S1). Moreover, cells were marked by expression of early neural crest/dorsal neural tube/BMP-TGFβ-related transcripts (e.g. *NR2F1/2*, *TGFBI*, *TGFB2*, *BMP6*, *ID4*, *BMPR1B*) (Frith et al., 2018; Kee and Bronner-Fraser, 2001; Lee et al., 1998; Rada-Iglesias et al., 2012), consistent with a pro-dorsalising role of WNT and FGF signalling pathways and in line with our previous work showing that hPSC-derived NMP-like cultures contain trunk neural crest precursors (Frith et al., 2018) (Fig. 2E, Fig. S2B, Table S1). Addition of exogenous RA, which has been shown to promote neural differentiation of NMPs and their pre-neural derivatives, both *in vivo* and *in vitro* (Diez del Corral et al., 2002, 2003; Gouti et al., 2017, 2014; Verrier et al., 2018), in the presence of FGF2 and CHIR, boosted the expression of the definitive neural marker *PAX6* and diminished the levels of the NMP/pre-neural marker *NKX1-2* without affecting *CDX2* expression (Fig. S2C). Finally, although induction of HOX transcripts (especially those belonging to the *HOXB* cluster) was initiated in D3 NMP-like cells, their levels continued to be upregulated so that by D7 of differentiation most

members of PG(1-9) were highly expressed (Fig. 2F). Collectively, these data indicate that a combination of WNT and high FGF signalling activities steer human NMP-like cells predominantly toward a pre-neural/early neural state exhibiting dorsal neural tube features while simultaneously promoting a posterior axial identity.

Efficient induction of a ventral spinal cord neurectoderm from NMP-like cells requires combined BMP-TGFβ signalling pathway inhibition

We next tested culture conditions for the efficient ventralisation of pre-neural/early spinal cord progenitors derived from human NMP-like cells following WNT and FGF stimulation. *In vivo*, the ventral neural tube, where MNs and their progenitors arise, is patterned by a gradient of notochord/floor plate-derived SHH signalling activity (reviewed by Sagner and Briscoe, 2019). Therefore, we initially treated hPSC-derived NMP-like cells with WNT-FGF agonists and RA to induce early posterior neurectoderm, as described above (Fig. 2, Fig. S2C), together with the SHH signalling pathway agonists smoothened agonist (SAG) and purmorphamine to promote ventralisation (Amoroso et al., 2013) (Fig. 3A). We also
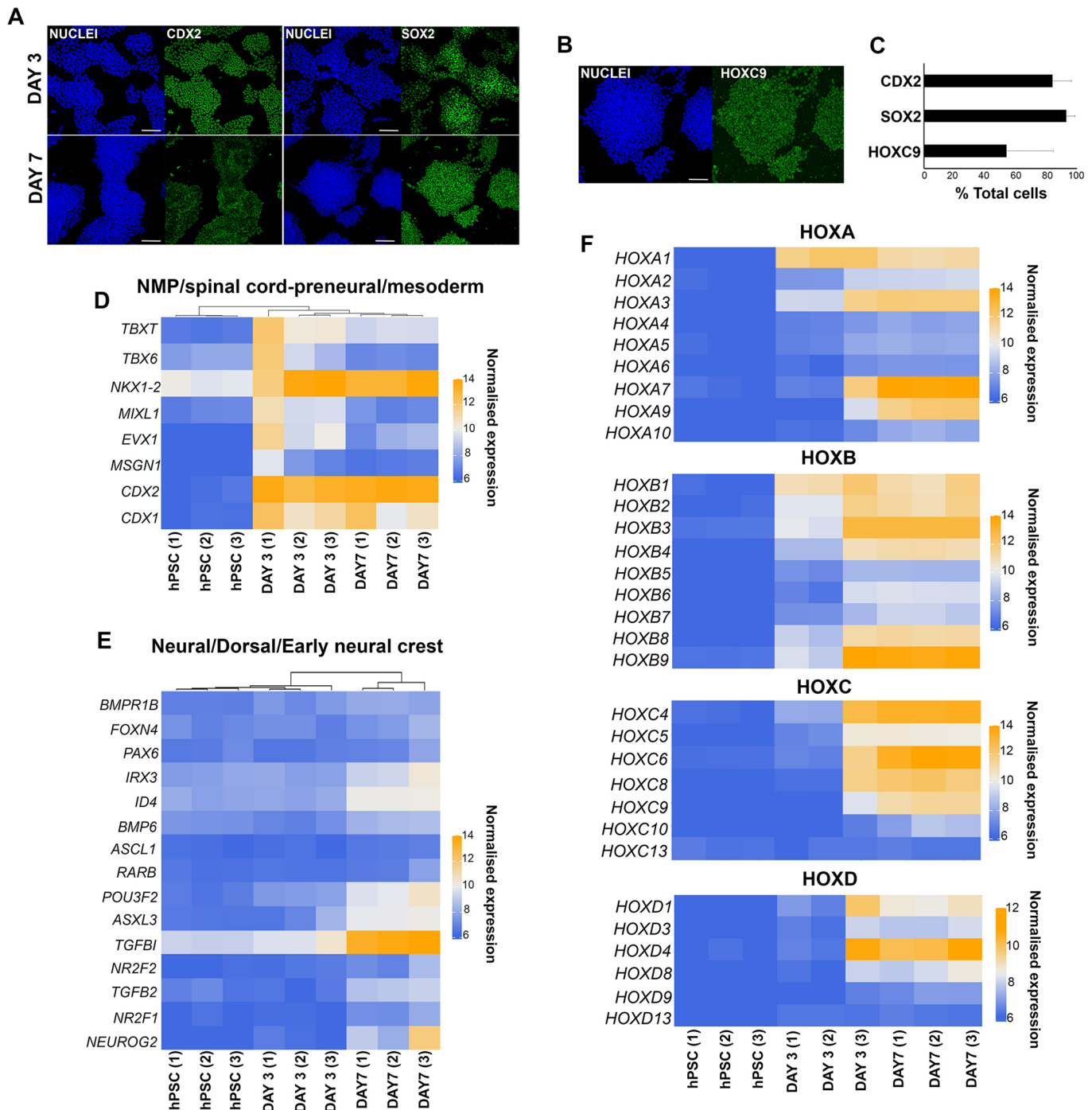
Fig. 2. WNT-FGF-mediated induction of pre-neural/early neural progenitors from human NMP-like cells. (A) Immunofluorescence analysis of the expression of CDX2 and SOX2 in D3 (i.e. NMP-like cells) and D7 pre-neural/early neural progenitors following differentiation of hPSCs in the presence of 3 μM CHIR and 100 ng/ml FGF2 as described in Fig. 1A. Scale bars: 100 μm. (B) Immunofluorescence analysis of the expression of HOXC9 expression in D7 WNT-FGF-induced pre-neural/early neural progenitors following differentiation of hPSCs. Scale bar: 50 μm. Note that the image corresponds to the same D7 cultures stained for SOX2 in Fig. 2A following double immunostaining. (C) Quantification of CDX2^{+}, SOX2^{+} and HOXC9^{+} cells in D7 WNT-FGF-induced pre-neural/early neural progenitor cultures following immunostaining and image analysis. Average percentages of cells over total numbers are depicted. The data in the graph were obtained after scoring 5-20 random fields per experiment (three independent replicates) and the error bars represent the variation (s.d.) across all fields and experiments. (D) Heatmap showing the normalised expression values of NMP/early spinal cord/paraxial mesoderm transcripts in three independent hPSC, NMP-like (day 3) and WNT-FGF-induced pre-neural/early neural progenitor (day 7) sample replicates. Numbers in brackets indicate individual replicates. Values were variance stabilised using the vst function in DESeq2. (E) Heatmap showing the normalised expression values of representative neural/dorsal/BMP/TGFβ-associated markers in three independent hPSC, NMP-like (day 3) and WNT-FGF-induced pre-neural/early neural progenitor (day 7) sample replicates. Numbers in brackets indicate individual replicates. Values were variance stabilised using the vst function in DESeq2. (F) Heatmaps showing the normalised expression values of HOX transcripts belonging to different clusters in three independent hPSC, NMP-like (day 3) and WNT-FGF-induced pre-neural/early neural progenitor (day 7) sample replicates. Numbers in brackets indicate individual replicates. Values were variance stabilised using the vst function in DESeq2.

included a BMP pathway inhibitor (LDN 193189) during the initial induction of NMP-like cells from hPSCs (D0-3) to suppress the emergence of neural crest cells, as we previously showed that endogenous BMP activity during that stage can promote early neural crest features at the expense of central nervous system neural cells (Frith et al., 2018). Following WNT-FGF agonist removal after D10, cells were further cultured in neurotrophic media containing BDNF, GDNF, L-ascorbic acid and the NOTCH/γ-secretase inhibitor DAPT (after D14), to promote exit from a progenitor state and MN maturation as described previously (Maury et al., 2015) (Fig. 3A). This approach [tested in both human induced PSC (hiPSC) and human embryonic stem cell (hESC) lines] gave rise to cultures expressing ventral spinal cord/MN progenitor-associated transcription factors OLIG2, NKX6-1 and NKX6-2 (Briscoe et al., 2000; Lu et al., 2002; Novitch et al., 2001; Sagner et al., 2018; Sander et al., 2000; Takebayashi et al., 2002; Vallstedt et al., 2001) from around D14 (Fig. 3B,D, black bars), as well as the definitive MN markers ISL1/2 (Ericson et al., 1992; Thaler et al., 2004) and MNX1 (Arber et al., 1999; Thaler et al., 1999) around D24 (Fig. 3B, D, black bars; Fig. 3C). Differentiating cells retained high levels of HOXC9 expression (~80% of total) (Fig. 3D) indicating the stable acquisition of a posterior axial identity. Together, these results suggest that WNT-FGF-RA-induced, NMP-derived early spinal cord progenitors can be ventralised and give rise to posterior MNs. However, both D14 and D24 cultures were found to be heterogeneous containing only low numbers of OLIG2$^+$ MN progenitors and ISL1/2$^+$ or MNX1$^+$ MNs (≤5% of total), respectively (Fig. 3C,D).

The low efficiency of our MN differentiation protocol prompted us to analyse in detail the composition of the 'contaminating' non-MN cell types present in the cultures. Given the reported propensity of NMP-like cells to generate neural crest (Frith et al., 2018; Hackland et al., 2019) and the dorsal character of NMP-derived early neurectoderm (Fig. 2D), we tested the presence of dorsal neural cell types/prospective neural crest during MN differentiation. Indeed, qPCR analysis of D8, D14 and D24 hiPSC- and hESC-derived cultures showed that these exhibited very high expression of the dorsal neural tube/neural plate border-early neural crest markers PAX3 and MSX1 (Goulding et al., 1991; Timmer et al., 2002) (Fig. 3B, Fig. S3A, black bars). This finding indicates that stimulation of SHH signalling alone was not sufficient to eliminate the dorsal bias of human NMP neural derivatives and drive homogeneous ventralisation/induction of MNs.

We hypothesised that active repression of dorsalisation may be required in order to block the induction of unwanted dorsal neural/neural crest cells. To this end, we tested the effect of inhibitors of established dorsalising signalling pathways such as BMP and TGFβ (Fig. 3A), components of which were also found to be enriched in D7 WNT-FGF-RA-induced neurectoderm (Fig. 2E). Although BMP antagonism alone was found to be effective (Fig. 3B,D, Fig. S3A, dark blue versus black bars), inclusion of inhibitors of both BMP and TGFβ pathways, during early neural differentiation of hPSC-derived NMP-like cells (D3-10), proved to be the optimal approach for eliminating the expression of PAX3 and MSX1 between D8-24 (Fig. 3B, Fig. S3A, light blue bars) and improving the induction of ventral/MN progenitor markers NKX6.1/NKX6.2 and ISL1/MNX1 at D14 and 24, respectively (Fig. 3B, light blue bars). A similar positive effect of dual BMP-TGFβ inhibition on the overall numbers of OLIG2, ISL1/2 and MNX1 protein-expressing cells was also observed (6- to 10-fold increase compared with untreated controls while remaining positive for HOXC9) (Fig. 3C; Fig. 3D, light blue bars). We conclude that the simultaneous blocking of BMP/TGFβ

signalling activities, combined with stimulation of SHH signalling, drives efficient acquisition of a ventral identity by NMP-derived posterior spinal cord progenitors in vitro, possibly by eliminating the specification of dorsal neural/prospective neural crest cells.

Dual BMP-TGFβ signalling inhibition has been previously shown to promote efficient neural induction from NMP-like cells (Rayon et al., 2020; Verrier et al., 2018). Thus, we also examined whether the positive effect we observed on MN generation yields, following treatment with BMP-TGFβ inhibitors, may be also a result of augmented neural differentiation. To this end, we assessed the number of neural progenitors emerging at an early stage (D8) during differentiation of NMP-like cells under different combinations of inhibitor treatments. We found that the combined attenuation of BMP-TGFβ signalling leads to a decrease in the total number of SOX2$^+$ early neural progenitor cells (from 90% to ~70%) (Fig. S3B, light blue bars) and a concomitant increase in the fraction of cells expressing the later neural progenitor marker SOX1 (Wood and Episkopou, 1999; Zhang et al., 2010) (Fig. S3C). This finding suggests that blocking of BMP-TGFβ activities enhances neural differentiation of SOX2$^+$ early spinal cord progenitors potentially by restricting the emergence of neural crest cells as mentioned earlier and also accelerating their transition toward a 'later' neural fate in line with previous reports showing that these signalling pathways are crucial for the temporal control of neurogenesis (Dias et al., 2014; Ma et al., 2020; Sagner et al., 2020 preprint).

Generation of posterior MNs from hPSC-derived NMP-like cells
Using the above findings, we established an improved protocol for the in vitro generation of posterior MNs. This relies on the induction of posterior neurectoderm (via WNT-FGF-RA stimulation/BMP-TGFβ inhibition), which is simultaneously ventralised at high efficiency (SHH stimulation/BMP-TGFβ inhibition), from NMP-like cells, followed by culture in neurotrophic media (BDNF, GDNF, L-ascorbic acid, DAPT) as described above (Fig. 3A, Fig. S5A). We tested this protocol in four different hPSC lines [two hiPSCs (SFCi55-ZsGr, MIFF1) and two hESCs: (H7 and H9); Desmarais et al., 2016; Lopez-Yrigoyen et al., 2018; Thomson et al., 1998]. We found that in all lines tested, early ventral spinal cord/MN progenitor-related transcripts (NKX6-1, OLIG2) were induced between D7-14 and, concurrently, a wave of expression of committed MN markers (MNX1, ISL1) occurred primarily during the D14-24 time window (Fig. 4A). The transcript levels of the early spinal cord progenitor marker CDX2 became extinct by D24 and posterior HOX transcripts belonging to PG(6-10) were highly expressed throughout differentiation (Fig. 4A). It should be noted that the temporal expression dynamics and extent of induction of some of these genes varied between different hPSC lines (Fig. 4A), possibly reflecting the well-described transcriptional and epigenetic differences of hPSC lines that affect their differentiation potential (Bock et al., 2011; International Stem Cell, 2018; Koyanagi-Aoi et al., 2013; Nishizawa et al., 2016). Collectively, these results indicate that our protocol promotes the progressive and robust induction of ventral spinal cord progenitors and MNs exhibiting a posterior axial identity.

To verify the identity of the differentiating cells, we carried out antibody staining and fluorescence microscopy. These analyses confirmed that D14 cultures were predominantly HOXC9$^+$ (~80% of total cells) and consisted of a mix of OLIG2$^+$ MN progenitors (35-70% of total cells depending on the hPSC line) and ISL1/2-neurofilament heavy chain (NF-H) double-positive MNs (~30-40% of total cells depending on the hPSC line) (Figs 3D and 4B, Fig. S4A,C). At D24, we observed the emergence of a considerable
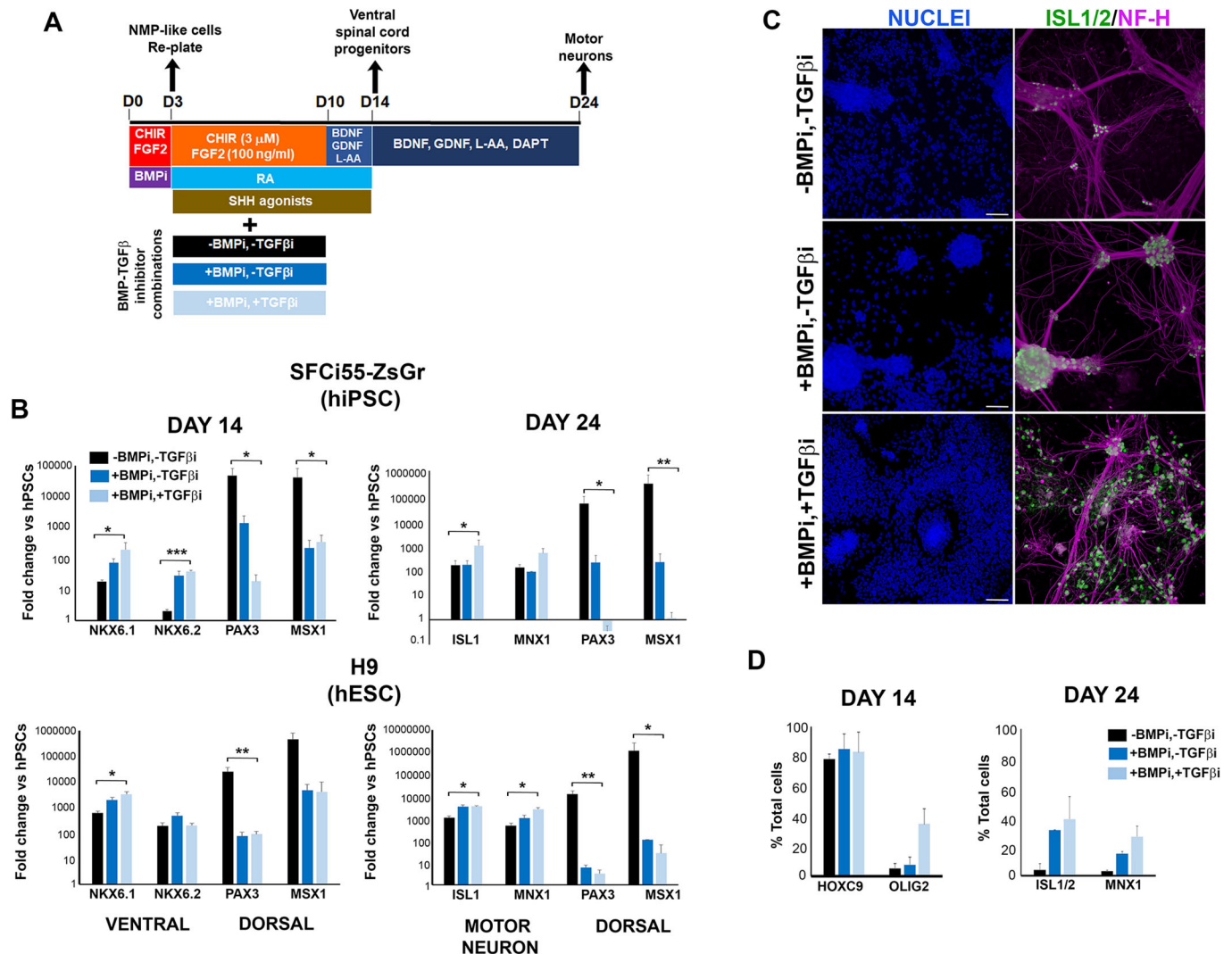
Fig. 3. Combined TGFβ/BMP signalling inhibition drives efficient induction of a ventral identity in NMP-derived neurectoderm. (A) Diagram depicting the culture conditions employed and tested for the generation of MN progenitors (D14) and MNs (D24) from hPSC-derived NMP-like cells. L-AA, L-ascorbic acid. (B) qPCR expression analysis of indicated dorsal, ventral and MN markers in the absence (black bars) and presence of BMP only (dark blue bars) or TGFβ and BMP (light blue bars) inhibitors (i) at different time points during the differentiation of NMP-like cells to MNs as described in A. Results are shown for a hiPSC (top) and a hESC (bottom) line. Error bars represent s.d. (*n*=3) *P<0.05, **P<0.005, ***P<0.0005 (paired *t*-test). (C) Immunofluorescence analysis of the expression of the MN marker ISL1/2 together with the pan-neuronal marker neurofilament heavy chain (NF-H) in D24 cultures following differentiation of hPSCs in the absence and presence of BMP only or TGFβ and BMP inhibitors. Scale bars: 100 μm. (D) Quantification of cells marked by expression of the indicated proteins at D14 and D24 after MN differentiation of hPSCs in the absence (black bars) and presence of BMP only (dark blue bars) or TGFβ and BMP (light blue bars) inhibitors and following immunofluorescence and image analysis. The data in the graph were obtained after scoring: at D14, two random fields per experiment (two independent replicates) (for −TGFβi, −BMPi and −TGFβi, +BMPi) or four random fields per experiment (two independent replicates) (for +TGFβi, +BMPi); at D24, three random fields per experiment (two independent replicates) (for −TGFβi, −BMPi and −TGFβi, +BMPi) or five random fields per experiment (two independent replicates) (for +TGFβi, +BMPi). Error bars represent s.d.

number of three-dimensional clusters consisting of ISL1/2+ cells (∼30-60% of total cells depending on the hPSC line) and/or MNX1+ cells (25-35% of total cells) forming networks via NF-H+ neuronal connections (Figs 3C,D and 4C,D, Fig. S4B). Moreover, we found that D14 MN progenitor/MN cultures retained the expression of all appropriate markers and could be differentiated into more mature MNs following freezing and thawing (Fig. S4D). Taken together, these data suggest that our protocol can be applied to various hPSC lines to generate considerable numbers of posterior MN progenitors/MNs via an NMP-like intermediate.

We next compared our posterior MN differentiation strategy (i.e. 4-day culture of hPSC-derived NMP-like cells in the presence of WNT-FGF agonists alongside SHH stimulation/BMP-TGFβ

inhibition prior to addition of neurotrophic media; Fig. 3A; Fig. S5A, 'Long WNT-FGF') to the conventional NMP-based approach for generating MNs, which typically relies on culture of NMP-like cells in BMP-TGFβ inhibitors, RA, SHH agonists followed by neurotrophic media (Gouti et al., 2014; Rayon et al., 2020; Verrier et al., 2018) (Fig. S5A, 'Short WNT-FGF'). We found that, in line with previous reports (Estevez-Silva et al., 2018; Rayon et al., 2020; Verrier et al., 2018), the latter promotes mainly cells of a brachial character, indicated by high levels of *HOXB6* and *HOXB8* transcripts (Asli and Kessel, 2010; Lacombe et al., 2013) whereas, as described above, our protocol yields cultures marked by higher levels of posterior brachial/thoracic/lumbar spinal cord-associated transcripts (*HOXC8-10*) (Fig. S5B) as well as HOXC9
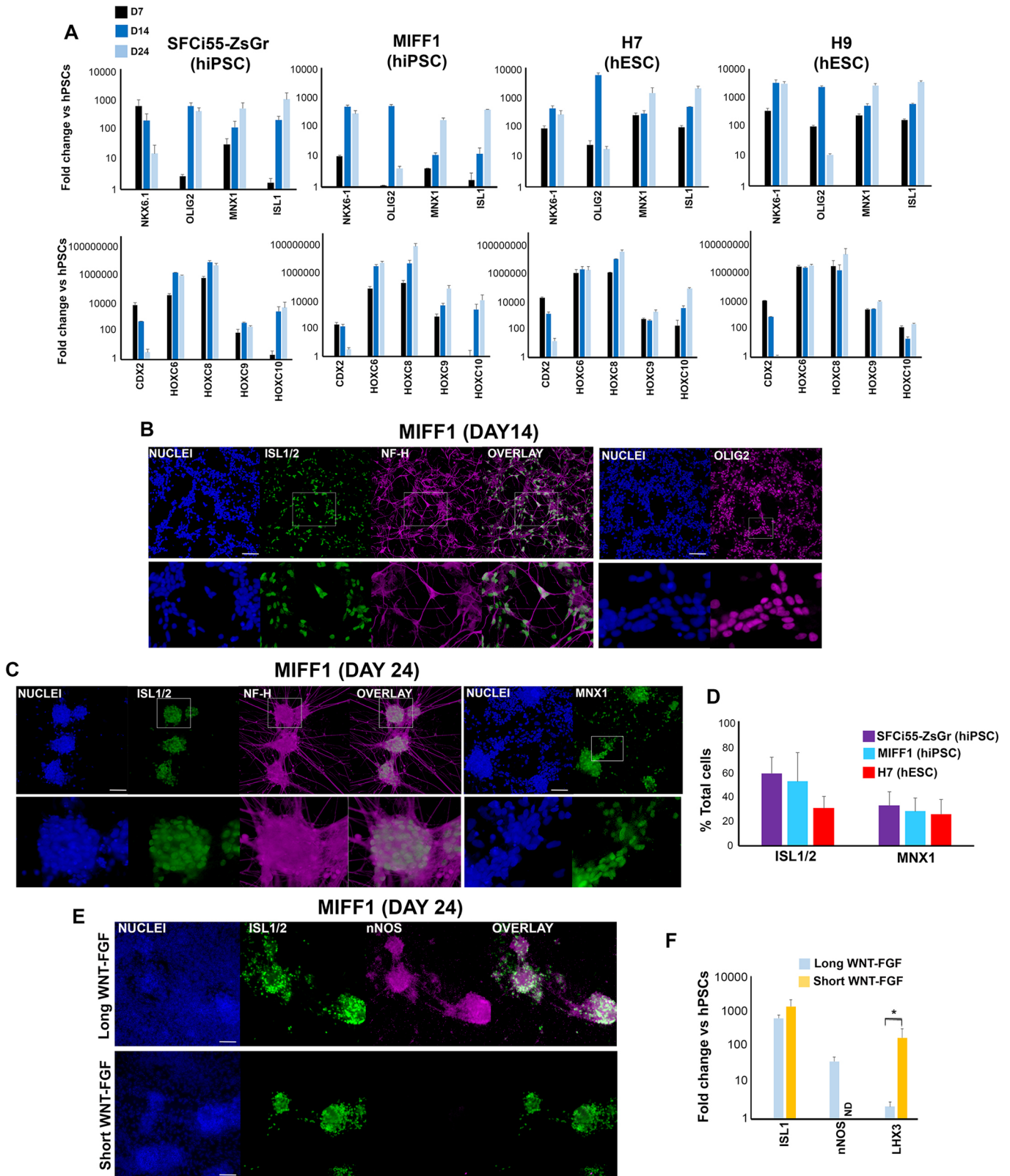
Fig. 4. See next page for legend.

protein (Fig. S5C). An MN column that is present exclusively at the thoracic axial level is the preganglionic motor column (PGC), which innervates sympathetic ganglia and is specified through the action of HOXC9 (Jung et al., 2010). We speculated that the lower number of MNX1^{+} cells in our D24 cultures (Fig. 4D), compared with those obtained with protocols generating MNs of a more anterior axial identity (Du et al., 2015; Maury et al., 2015), in combination with the observed high levels of HOXC9 positivity (Fig. 3D, Figs S4C

Fig. 4. Generation of posterior MN progenitors and MNs from hPSCs.
(A) qPCR expression analysis of the indicated MN progenitor/MN markers
(top) and posterior HOX transcripts (bottom) at different time points during the
differentiation of various human induced pluripotent (hiPSC) and embryonic
stem cell (hESC) lines to MNs after re-plating of NMP-like cells in WNT-FGF
and in the presence of BMP/TGFβ inhibitors (see Fig. 3A, Fig. S5A). Error bars
represent s.d. (n=3). (B) Immunofluorescence analysis of the expression of the
MN marker ISL1/2 together with the pan-neuronal marker neurofilament heavy
chain (NF-H), and the MN progenitor marker OLIG2 in day 14 cultures
differentiated from MIFF1 hiPSCs as described in A. Magnified regions
corresponding to the boxed areas are also shown. (C) Immunofluorescence
analysis of the expression of the MN marker ISL1/2 and NF-H in day 24
cultures differentiated from MIFF1 hiPSCs as described in A. Magnified
regions corresponding to the boxed areas are also shown. (D) Quantification of
cells marked by expression of MN-associated proteins at D24 after
differentiation of the indicated hPSC lines as described in A and following
immunofluorescence and image analysis. The data in the graph were obtained
after scoring seven random fields per experiment (three independent
replicates). Error bars represent s.d. (E) Immunofluorescence analysis of the
expression of the PGC/MN markers nNOS and ISL1 in day 24 MN cultures
generated using MIFF1 hiPSCs as described in A (i.e. after re-plating of NMP-
like cells either in WNT-FGF, RA and BMP/TGFβ inhibitors; 'Long WNT-FGF')
or after re-plating of NMP-like cells in RA and BMP/TGFβ inhibitors ('Short
WNT-FGF') (see Fig. S5A). (F) qPCR expression analysis of the indicated MN
columnar identity markers in day 24 MN cultures generated in parallel as
described in E (see Fig. S5A). Error bars represent s.d. (n=3). ND, not
detected. *P<0.05 (paired t-test). Scale bars: 100 µm.

and S5C), is likely to reflect the presence of PGC MNs, which are
marked by the absence of MNX1 expression (William et al., 2003).
To confirm this further, we examined the expression of the PGC-
specific marker neuronal nitric oxide synthase (nNOS), (Wetts and
Vaughn, 1994) and found that D24 ISL1/2$^+$ MN clusters, generated
using our protocol, exhibited nNOS expression both at the protein
and transcript level (Fig. 4E,F, Fig. S5D; 'Long WNT-FGF'). In
contrast, no nNOS expression was observed in MN cultures
generated using the conventional NMP-based approach (Fig. 4E,
F, Fig. S5D; 'Short WNT-FGF'). The latter gave rise to MNs
expressing high levels of ISL1/2 as well as LHX3, a marker of
median motor column (MMC) MNs (Tsuchida et al., 1994), which
are present at all A-P levels in vivo and project dorsally to axial
muscles (Fig. 4E,F, Fig. S5D, 'Short WNT-FGF'). Together, these
findings indicate that our differentiation strategy presents an
efficient route toward the production of thoracic MNs of a PGC
character in contrast to previous NMP-based approaches, which
tend to generate more anterior brachial/MMC MNs.

Characterisation of human NMP-derived posterior MNs

We next tested the ability of posterior D14 MN progenitors/early
MNs, produced from hPSC-derived NMP-like cells using our
protocol, to integrate within the embryonic spinal cord and establish
neuronal projections toward muscles in vivo. Such a population
could be a promising platform for the development of cell therapy-
based strategies against ALS and spinal cord injury (Kadoya et al.,
2016; Kondo et al., 2014; Kumamaru et al., 2018; Zalfa et al., 2019).
We employed cells derived from SFCi55-ZsGr hiPSCs, which carry a
constitutive ZsGREEN fluorescent reporter (Lopez-Yrigoyen et al.,
2018), and transplanted them into chick embryos, a well-established
method for testing the developmental potential of PSC-derived cells
in an embryonic environment (Frith et al., 2018; Peljto et al., 2010;
Wichterle et al., 2002) (Fig. S6A). Donor cells were grafted to the
posterior open neural tube of Hamburger and Hamilton (HH) stage
10-13 chick embryos, i.e. a site that gives rise to brachial/thoracic
regions of the spinal cord (Fig. 5A). This host site can therefore be
defined as 'homotopic' in terms of axial identity, for the posterior MN

progenitors/MN donor cells. After incubation, host embryos were
harvested at HH26-30. Of the 30 embryos examined, 22 showed no
developmental abnormalities and 11 of these contained ZsGREEN$^+$
cells located within the thoracic spinal cord between the forelimb and
hindlimb levels, as revealed by whole-mount imaging (Fig. 5A).
Embryos were sectioned (n=8) and the incorporation/differentiation
of hPSC-derived fluorescent cells was assessed following
immunostaining and fluorescence microscopy.

We found that the human donor cells (6/8 embryos) integrated
well within the ventral part of the neural tube encompassing the MN
progenitor domain (Fig. 5Bi, green arrowheads) and expressed
ISL1/2, HOXC9 and NF-H (Fig. S6B,C) consistent with thoracic
MN differentiation, although OLIG2$^+$ donor cells were also
detected within donor cell clumps (Fig. S6B) indicating the
presence of more immature MN progenitors as well. Importantly,
donor ZsGREEN$^+$ cells projected axons in a manner similar to
endogenous host MNs: (1) in 6/8 embryos, ZsGREEN-positive
axons exited the neural tube via the MN ventral root (e.g. Fig. 5Bi;
yellow arrowheads); (2) in many cases (4/8 embryos), sections
adjacent to those with the main bulk of integrated cells revealed
donor cell-derived axons exiting the neural tube and projecting
along the MN ventral root towards muscle target cells, following the
endogenous pathway (Fig. 5Bii,Biii; white arrowheads); (3) in 2/8
embryos, we found ZsGREEN$^+$ axons exiting the ventral neural
tube and projecting toward the sympathetic chain ganglia, a feature
of PGC MNs emerging at the thoracic levels of the spinal cord
(Fig. 5Biii; pink arrowheads).

Interestingly, we also observed donor cell projections toward (and
sometimes into/beyond) the dorsal root ganglia (DRG) following
exit via the ventral root (5/8 embryos; Fig. 5Bii,Biii; blue
arrowheads). Collectively, these findings suggest that thoracic
MN progenitors/MNs generated from hPSC-derived NMP-like can
integrate efficiently into the posterior embryonic spinal cord
following homotopic transplantation to the chick embryo, and can
establish appropriate neuronal projections.

We next examined the influence of axial identity on the
electrophysiological properties of spinal cord MNs by comparing
our posterior MN cultures with their anterior counterparts, as the
firing rate of various MN subtypes has been linked to differential
vulnerability to ALS (Brockington et al., 2013; Nijssen et al., 2017).
To this end, we generated MNs of a hindbrain/cervical character
using an established differentiation strategy: hPSCs were first
treated with TGFβ/BMP signalling inhibitors to induce an anterior
Hox-negative neurectodermal intermediate, and then with RA/SHH
agonists to promote posteriorisation/ventralisation (Amoroso et al.,
2013; Chambers et al., 2009; Wichterle et al., 2002) (Fig. S7A).
Following culture in neurotrophic media, the resulting cultures
exhibited mixed expression of MN progenitor (NKX6.1/OLIG2)
and committed MN (ISL1) markers at D14 of differentiation
(Fig. S7B), whereas at D24 they consisted mainly of ISL1/2$^+$
clusters with NF-H$^+$ neuronal projections (Fig. S7C).The cells were
also found to exhibit high levels of HOX PG(1-5) gene expression
and low levels of MNX1 as well as no/very low CDX2 and HOX
PG(6-10) gene expression, confirming their hindbrain/cervical axial
identity (Fig. S7B). Whole-cell current clamp recordings revealed
that both these anterior MNs and their posterior thoracic counterparts,
generated using our protocol, exhibited comparable action potential
firing rates (Fig. 5C). These were similar to those reported for in vivo-
transplanted mouse PSC-derived MNs (Soundararajan et al., 2006)
and rat embryonic MNs (Alessandri-Haber et al., 1999). Together,
these data indicate that anterior and posterior hPSC-derived MNs are
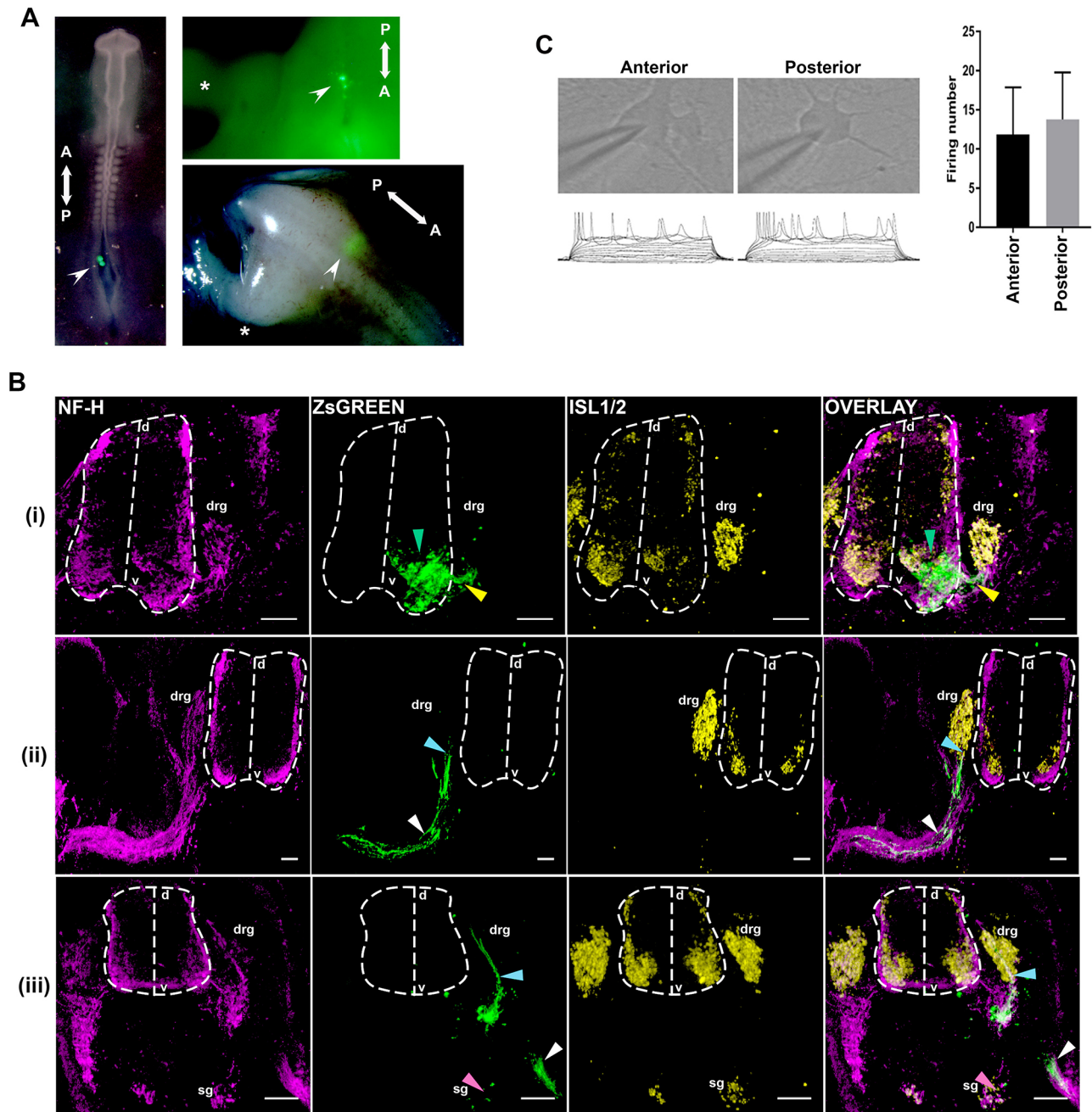likely to be equivalent in terms of electrophysiology.

Fig. 5. Testing the functionality of hPSC-derived posterior MNs. (A) Whole-mount embryo images showing the engrafted ZsGREEN+ donor cells (arrowheads) straight after transplantation (left) and prior to sectioning, following host embryo incubation (right). Asterisks indicate the position of the limbs. A, anterior; P, posterior. (B) Representative immunofluorescence analysis images of ZsGREEN, NF-H and ISL1/2 expression marking donor human cells, neuronal projections and dorsal root ganglion (drg)/MN-containing ventral neural tube/sympathetic ganglia (sg), respectively, in sections of HH26-30 chick embryos grafted with hPSC-derived ZsGREEN+ posterior D14 MN progenitor/MN cultures. Dashed outlines mark the boundaries of the neural tube. d, dorsal; v, ventral. Green arrowheads mark cell integration within the ventral MN progenitor domain. Yellow arrowheads mark ZsGREEN-positive axons exiting the neural tube via the MN ventral root. White arrowheads mark ZsGREEN-positive axons exiting the neural tube and projecting along the MN ventral root towards muscle target cells, following the endogenous pathway. Pink arrowheads mark ZsGREEN+ cells within the sympathetic chain ganglia. Blue arrowheads mark donor cell projections toward the dorsal root ganglia. Scale bars: 100 μm. (C) Firing rate of anterior and posterior hPSC-derived MNs. Whole-cell current clamp recordings were performed at room temperature and injected with 15 steps of currents from −80 pA to +60 pA (10 pA increase for each step). Representative traces of each group are shown on the left. Total firing number of each neuron with magnitude of 20 mV or higher were counted for analysis. Analysis results are shown on the right (number of recorded neurons=14, mean±s.e.m.; one-way ANOVA Tukey's multiple comparison test, no significant difference between the two groups).

DISCUSSION

Here, we have described an optimised protocol for the generation of functional posterior MNs from various hPSCs via the induction of NMP-like cells. Our work addresses a major gap in conventional hPSC differentiation strategies, namely the low efficiency of most protocols in generating thoracic spinal cord cells and MNs. It therefore opens new avenues toward the development of novel regenerative medicine and disease modelling approaches that rely

on the induction of defined regional identities *in vitro*. Our approach gives rise to considerable numbers of OLIG2$^+$ MN progenitors and ISL1/2$^+$ MNs (up to 70% and 60% of total cells, respectively), which also express high levels of HOX PG(6-9) genes/nNOS but do not express *LHX3*, thus reflecting their posterior brachial/thoracic axial identity. These yields represent an improvement over previous protocols for the production of thoracic/PGC MNs from adherent human NMP-like cells (Estevez-Silva et al., 2018; Gouti et al., 2014; Lippmann et al., 2015; Rayon et al., 2020; Verrier et al., 2018), and this is, to our knowledge, the first time that the NMP-based, *in vitro* generation of thoracic human MNs is characterised in detail and across different hPSC lines. The detection of *HOXC10* transcripts in our MN cultures also indicates the presence of cells corresponding to the lumbar level of the spinal cord, although these are likely to represent a minor entity given that our protocol does not involve the addition of the TGFβ family member GDF11, an established driver of lumbosacral axial identity in hPSC-derived MNs (Lippmann et al., 2015; Mouilleau et al., 2020 preprint).

We found that the posterior MNs produced using our approach exhibit electrophysiological properties that are crudely similar to those shown by hPSC-derived MNs of a hindbrain/anterior spinal cord character: further comparative characterisation of their electrophysiological properties is now required to compare the two populations thoroughly. Moreover, following transplantation to the posterior spinal cord of chick embryos, our posterior MNs showed hallmarks of their endogenous *in vivo* counterparts, i.e. expression of ISL1/2 and HOXC9 and establishment of NF-H-positive axonal projections exiting, via the ventral root, toward target muscles/sympathetic ganglia. Interestingly, grafted donor cells also tended to form neuronal projections toward the DRG, a pattern that has been previously observed with grafts of PSC-derived MNs of a more anterior (hindbrain/cervical/anterior brachial) axial identity (Amoroso et al., 2013; Soundararajan et al., 2006), indicating that such cells may also be present in our cultures. Alternatively, this may reflect low levels of CXCR4 expression in our donor D14 posterior MN progenitor/MN cultures due to incomplete differentiation, as similar projections of ventral spinal cord MNs toward the DRG have been previously reported in *Cxcr4* mutant mice (Lieberam et al., 2005).

Our data show that distinct levels of WNT and FGF signalling activities steer hPSC-derived NMP-like cells toward their immediate derivatives, paraxial mesoderm or pre-neural/early neural cells. The transition to the latter entity occurs via a pre-neural NKX1-2$^+$SOX2$^+$CDX2$^+$ state and day 7 WNT-FGF-induced cultures are composed mainly of a mixture of such pre-neural and early neural progenitors, which are likely to exhibit neural crest-forming potential. Their emergence is likely to be driven directly by FGF and WNT signalling, as these pathways have been shown to promote specification and maintenance of early posterior progenitors in the caudal lateral epiblast/pre-neural tube *in vivo* (Diez del Corral et al., 2002, 2003; Mathis et al., 2001; Nordstrom et al., 2006; Olivera-Martinez et al., 2014; Olivera-Martinez and Storey, 2007; Storey et al., 1998; Takemoto et al., 2006). It should be noted that these results are in agreement with a recent report showing that prolonged cultured of hPSC-derived NMP-like cells promotes their transition toward a CDX2$^+$SOX2$^+$ pre-neural/early spinal cord, neural crest-potent progenitor state (Cooper et al., 2020 preprint).

Previous findings have suggested that spinal cord neurectoderm can be induced by addition of RA to WNT-FGF-induced hPSC-derived NMP-like cells: the longer the duration of WNT-FGF treatment during NMP induction, the more posterior the axial identity of their RA-induced neural derivatives (Lippmann et al., 2015). Similarly, we show that sequential HOX gene activation, and hence the acquisition of a posterior axial identity, is a function of the duration of WNT-FGF stimulation. However, we also found that progressive HOX gene induction takes place during the transition of NMP-like cells toward a pre-neural/early neural state rather than within a homogeneous TBXT$^+$SOX2$^+$ population maintained by continuous WNT-FGF treatment. Collectively, these findings suggest that WNT and FGF stimulation can 'program' a posterior axial identity (marked by posterior HOX gene expression) and further work is required to decipher how this is coupled to the induction of distinct NMP-derived lineages under the influence of the same signalling pathways.

The simultaneous induction of both a posterior axial and early neural identity, following WNT-FGF treatment of human NMP-like cells, is also marked by upregulation of dorsal neural tube markers and high activity of dorsalising BMP/TGFβ signalling pathways, in agreement with previous studies examining neural differentiation of hPSC-derived NMP-like cells (Denham et al., 2015; Frith et al., 2018; Hackland et al., 2019; Verrier et al., 2018). Both WNT and FGF pathways have been implicated in the promotion of a dorsal identity/repression of ventral patterning genes in neural cells (Alvarez-Medina et al., 2008; Diez del Corral et al., 2003; Muroyama et al., 2002) and our data suggest that their pro-dorsal effect may be mediated by activating downstream BMP and TGFβ signalling cascades. Furthermore, an increase in the expression of BMP and TGFβ pathway components has been reported to coincide with the onset of neuronal differentiation in the posterior neural tube during chick embryonic development (Olivera-Martinez et al., 2014). Hence, neuralisation and acquisition of a dorsal identity may be tightly coupled events during the generation of posterior neurectoderm *in vitro* and presage ventralisation. The latter can only be achieved by combining SHH agonist treatment with dual BMP-TGFβ signalling inhibition reflecting *in vivo* data showing that MN specification also depends on the activity of BMP-TGFβ signalling antagonists, such as noggin and follistatin (Liem et al., 2000; McMahon et al., 1998). Moreover, our data indicate that BMP-TGFβ inhibitors also improves differentiation efficiency by promoting neural differentiation of early SOX2$^+$ progenitors, potentially at the expense of neural crest specification and via the acceleration of the rate of neural commitment, as indicated by the increase in the number of SOX1$^+$ cells following treatment.

To date, it has been unclear whether the axial identity of neural derivatives of PSCs shapes their *in vivo* functionality, a crucial parameter to consider in the development of cell replacement therapies. Previous studies employing transplantation of PSC-derived neural progenitors of a presumed anterior axial identity have suggested that donor cells can survive, differentiate and even promote functional recovery in rodent disease and injury models within posterior spinal cord locations (Iwai et al., 2015; Kondo et al., 2014; Lu et al., 2017, 2014; Tsuji et al., 2010; Yohn et al., 2008). However, more recent data based on the use of both *in vivo*-and *in vitro*-derived neural progenitors have demonstrated that axial level homology between donor cell and spinal cord transplantation sites is a key factor for functional reconstitution in the injured spinal cord (Kadoya et al., 2016; Kumamaru et al., 2018). We envisage that the efficient generation of posterior spinal cord cells using our protocol will facilitate their direct functional comparison to their anterior counterparts, thus revealing whether the *in vivo* behaviour of hPSC-derived spinal cord cells is intrinsically determined by their *in vitro* axial identity, or plastic and influenced by extrinsic factors.

DEVELOPMENT

MATERIALS AND METHODS

Cell culture and differentiation

Use of hESCs has been approved by the Human Embryonic Stem Cell UK Steering Committee (SCSC15-23). The following hPSC lines were employed: SFCi55-ZsGr (Lopez-Yrigoyen et al., 2018), MIFF1 (Desmarais et al., 2016), H7 and H9 (Thomson et al., 1998).

All cell lines were tested mycoplasma negative. Cells were cultured in feeder-free conditions in Essential 8 (Thermo Fisher or made in-house) medium on laminin 521 (Biolamina). For NMP-like cell differentiation, hPSCs (60-80% confluency) were dissociated using PBS/EDTA and plated at a density of 63,000 cells/cm^2 on vitronectin (Thermo Fisher)-coated wells, directly into N2B27 medium containing CHIR99021 (3 µM, Tocris), FGF2 (20 ng/ml, R&D Systems), LDN-193189 (100 nM, Tocris) and ROCK inhibitor Y-27632 (10 µM, Adooq Biosciences) for the first day only. For early neurectoderm differentiation, day 3 hPSC-derived NMP-like cells were dissociated using Accutase and re-plated at a density of 37,500-86,000 cells/cm^2 on Geltrex (Thermo Fisher)-coated plates directly in N2B27 containing CHIR99021 (3 µM) and FGF2 (100 ng/ml) in the presence or absence of RA (0.1 µM, Tocris). For paraxial mesoderm differentiation, day 3 NMP-like cultures were treated with Accutase and re-plated at a density of 45,000 cells/cm^2 on Geltrex-coated plates in N2B27 containing FGF2 (40 ng/ml) and CHIR99021 (8 µM) for 2 days. For posterior MN differentiation, day 3 NMP-like cell cultures were treated with Accutase and re-plated at a density of 63,000 cells/cm^2 in N2B27 supplemented with CHIR99021 (3 µM), FGF2 (100 ng/ml), purmorphamine (1 µM, Sigma-Aldrich), SAG (0.5 µM, Tocris), all-trans RA (0.1 µM, Tocris), LDN-193189 (100 nM, Tocris), DMH1 (1 µM, Tocris), SB431542 (10 µM, Tocris) and ROCK inhibitor Y-27632 (10 µM) for the first day only, as indicated, on Geltrex-coated plates. Media were replaced every 2 days. Cells were re-plated on day 7 of differentiation using Accutase to lift and dissociate and then seeded at 86,000 cells/cm^2, on Geltrex- coated plates, in the same media as described above. At day 10 of differentiation, the media was changed to N2B27 supplemented with purmorphamine (1 µM), SAG (0.5 µM), all-trans RA (0.1 µM), BDNF (20 ng/ml, Peprotech), GDNF (20 ng/ml, Peprotech) and L-ascorbic acid (200 µM, Sigma-Aldrich) and replaced again at day 12. At day 14 of differentiation, cells were re-plated using Accutase and seeded at a density of 100,000 cells/cm^2 onto Geltrex-coated plates in N2B27 medium supplemented with BDNF (20 ng/ml), GDNF (20 ng/ml) and L-ascorbic acid (200 µM), DAPT (10 µM, Sigma-Aldrich), ROCK inhibitor Y-27632 (10 µM) for the first day only. Media were replaced every other day until day 24 or 36 of differentiation. For anterior MN differentiation, hPSCs (confluency of 60-80%) were seeded at 63,000 cells/cm^2, on Geltrex-coated plates, in N2B27 containing LDN-193189 (100 nM), SB431542 (10 µM) and ROCK inhibitor Y-27632 (10 µM) for the first day only. On day 3 of differentiation, cells were replaced at 63,000 cells/cm^2, on Geltrex coated plates, in N2B27 supplemented with LDN-193189 (100 nM), DMH1 (1 µM, Tocris), SB431542 (10 µM), purmorphamine (1 µM), SAG (0.5 µM), all-trans RA (0.1 µM) and ROCK inhibitor Y-27632 (10 µM) for the first day only. Media were re-placed at day 6 of differentiation. At day 7, cells were re-plated at a density of 86,000 cells/cm^2 on Geltrex-coated plates, in N2B27 supplemented with LDN-193189 (100 nM), SB431542 (10 µM), purmorphamine (1 µM), SAG (0.5 µM), all-trans RA (0.1 µM) and ROCK inhibitor Y-27632 (10 µM) for the first day only. At day 10, the media was changed to N2B27 supplemented containing purmorphamine (1 µM), SAG (0.5 µM), all-trans RA (0.1 µM), BDNF (20 ng/ml), GDNF (20 ng/ml) and L-ascorbic acid (200 µM) and replaced again at day 12. At day 14 differentiation, cells were re-plated using Accutase and seeded at a density of 100,000 cells/cm^2 onto Geltrex-coated plates in N2B27 medium supplemented with BDNF (20 ng/ml), GDNF (20 ng/ml) and L-ascorbic acid (200 µM,), DAPT (10 µM), ROCK inhibitor Y-27632 (10 µM) for 2 days. Media were replaced every other day until day 24.

RNA sequencing

Sample preparation

For RNA sequencing, we employed hESCs, D3 NMP-like cells and D7 CHIR-FGF-treated spinal cord progenitors. We used a genetically modified hESC line of H9 background also containing a tetracycline-inducible shRNA cassette against TBXT (Bertero et al., 2016). Cells were cultured in the absence of tetracycline and exhibited a differentiation behaviour comparable to unmodified controls (Bertero et al., 2016). Total RNA was harvested using the total RNA purification plus kit (Norgen BioTek) according to the manufacturer's instructions. Sample quality control, library preparation and sequencing were carried out by Novogene (http://en. novogene.com). Library construction was carried out using the NEB Next Ultra RNA Library Prep Kit and sequencing was performed using the Illumina NoveSeq platform (PE150).

Pre-processing of reads

FastQC v0.11.2 (https://www.bioinformatics.babraham.ac.uk/projects/fastqc/) was used for quality control of raw reads. Library adapters were trimmed using Trim Galore v0.4.0 (Babraham Bioinformatics - Trim Galore!; available at http://www.bioinformatics.babraham.ac.uk/projects/trim_galore/). Paired-end reads were aligned to the human reference genome assembly GRCh38 (Ensembl Build 79) using STAR v2.4.2a (Dobin et al., 2013) in the two-pass mode. Expected gene counts were extracted using RSEM v1.3.0 (Li and Dewey, 2011). Genes expressed in fewer than three samples or with total counts ≤5 among all samples were removed.

Differential expression and visualisation

Differential expression analysis was performed using the DESeq2 (v1.22.2) package (Love et al., 2014) in R (v3.5). Differentially expressed genes with log2FoldChange> |1| and Benjamini–Hochberg-adjusted $P<0.05$ were considered significant. Variance stabilising transformation (vst) (Anders and Huber, 2010) from the DESeq2 package was applied to the read counts for heatmap visualisation. Gene ontology analysis was carried out using the ToppGene suite (https://toppgene.cchmc.org/enrichment.jsp) (Chen et al., 2009).

Quantitative real time PCR

Total RNA from different samples was harvested using the total RNA purification plus kit (Norgen BioTek) according to the manufacturer's instructions. First strand cDNA synthesis was performed using the High-Capacity cDNA Reverse Transcription kit (Thermo Fisher) and random primers. Quantitative real-time PCR was carried out using the Applied Biosystems QuantStudio 12 K Flex thermocycler together with the Roche UPL system. Statistical significance was calculated using GraphPad Prism (GraphPad Software). See Table S2 for primer sequences.

Immunofluorescence

Cells were fixed for 10 min at 4°C in 4% paraformaldehyde (PFA) in PBS, then washed in PBST (PBS with 0.1% Triton X-100) and treated with 0.5 M glycine/PBST to quench the PFA. Blocking was then carried for 1-3 h in PBST supplemented with 3% donkey serum and 1% bovine serum albumin at room temperature or overnight at 4°C. Primary and secondary antibodies were diluted in PBST supplemented with 3% donkey serum and 1% bovine serum albumin. Cells were incubated with primary antibodies overnight at 4°C and with secondary antibodies at room temperature for 2 h in the dark. Cell nuclei were counterstained using Hoechst 33342 (1:1000, Thermo Fisher) and fluorescent images were taken using the InCell Analyser 2500 system (GE Healthcare). Chick embryos were fixed in 4% PFA for 2-3 h at 4°C and left in 30% sucrose solution overnight at 4°C. Chick embryos were mounted in OCT (VWR, 361603E) and transverse sections (15-20 µm) were taken using an OTF Bright Instruments cryostat. For immunostaining of sections, overnight incubation with the primary antibody at 4°C was followed by short washes in PBST, a 1 h incubation with the secondary antibody and further PBST washes. Slides were mounted in Fluoroshield with DAPI (Sigma-Aldrich) and imaged on the InCell Analyser 2200 (GE Healthcare) or a Widefield Fluorescent Inverted Microscope (Nikon Eclipse Ti-E). We used the following antibodies: anti-TBXT (1:200; ab209665, Abcam, RRID:AB_2750925), anti-SOX2 (1:200; ab92494, Abcam, RRID:AB_10585428), anti-CDX2 (1:200; ab76541, Abcam, RRID:AB_1523334), anti-ISL1/2 (1:100; DSHB #39.4D5, DSHB, RRID:AB_2314683)/(1:100; AF1837, R&D Systems, AB_2126324), anti-neurofilament, heavy chain (1:1000; ab8135, Abcam, RRID:AB_306298), anti-OLIG2 (1:200; AF2418, R&D Systems,

AB_2157554), anti- HOXC9 (1:50; ab50839, Abcam, RRID:AB_880494), anti-MNX1 (1:100; DSHB #81.5C10, DSHB, RRID:AB_2145209), anti-SOX1 (1:100; AF3369, R&D Systems, AB_2239879), anti-nNOS1 (1:100; 37-2800, Thermo Fisher, AB_2533308). Images were processed/enhanced using Photoshop and Fiji, employing identical brightness/contrast settings for images that were compared with each other. Nuclear segmentation followed by single-cell fluorescence quantification was performed either using CellProfiler (Carpenter et al., 2006) or a custom-made pipeline or as described previously (Osorno et al., 2012). Cells stained with secondary antibody only were used as a negative control to set a threshold fluorescence intensity. Following nuclear segmentation, the fluorescence intensity of each channel was masked back to nuclei and gave the number of positive (with fluorescence intensity greater than secondary only control) and negative cells per channel.

Chick embryo grafting
On day 13 of MN differentiation, cells were dissociated and plated at concentrations of 1000-5000 cells/cm^2 to form hanging drops in 20 µl of DMEM F12 media (Sigma) supplemented with N2 supplement (Thermo Fisher), MEM Non Essential Amino Acids (Thermo Fisher), Glutamax (Thermo Fisher). After 24 h of incubation at 37°C the cells generated clumps with a diameter of ∼50–100 mm. Fertilised Bovan brown chicken eggs (Henry Stewart and Co., Norfolk, UK) were staged according to Hamburger and Hamilton (Hamburger and Hamilton, 1951). Clumps were implanted in the neural tube of HH stage 10-13 chick embryos at the level of the newly developing somites. Following incubation, embryos we harvested at HH26-30.

Electrophysiology
Neurons were plated onto 13 mm coverslips at a density of 50,000 cells per coverslip. All recordings were performed at room temperature and all reagents for solutions were purchased from Sigma-Aldrich. Electrodes for patch clamping were pulled on a Sutter P-97 horizontal puller (Sutter Instrument Company) from borosilicate glass capillaries (World Precision Instruments). Coverslips were placed into a bath on an upright microscope (Olympus BX51) containing the extracellular solution at pH 7.4 composed of 150 mM NaCl, 5.4 mM KCl, 2 mM MgCl$_2$, 2 mM CaCl$_2$, 10 mM HEPES, 10 mM glucose, osmolarity∼305 mOsm/Kg. Whole-cell current clamp recordings were performed using an Axon Multi-Clamp 700B amplifier (Axon Instruments) using unpolished borosilicate pipettes placed at the cell soma. Pipettes had a resistance of 4-6 MΩ when filled with intracellular solution of 140 mM K$^+$-gluconate, 10 mM KCl, 1 mM MgCl$_2$, 0.2 mM EGTA, 9 mM NaCl, 10 mM HEPES, 0.3 mM Na$^+$-GTP and 3 mM Na$^+$-ATP adjusted to 298 mOsm/Kg at pH 7.4. For both solutions, glucose, EGTA, Na$^+$-GTP and Na$^+$-ATP were added fresh on each day of the experiment. To identify neurons present, cells were visualised using the microscope ×40 objective, and those with a triangular cell body and processes to indicate neuronal morphology were selected. To measure depolarised evoked action potential firing in the cells using a 15-step protocol for a duration of 500 ms, injecting current from −80 pA, every 10 pA. Recordings were acquired at ≥10 kHz using a Digidata 1440A analogue-to-digital board and pClamp10 software (Axon Instruments). Electrophysiological data were analysed using Clampfit10 software (Axon Instruments). Firing magnitude 20 mV and higher were included for analysis.

Author contributions
Conceptualization: M.W., A.T.; Validation: A.T.; Formal analysis: M.W., A.G., I.M., I.G., L.B., K.N., M.P., A.T.; Investigation: M.W., A.G., I.M., I.G., L.B., K.N., M.P., A.T.; Data curation: I.M., I.G.; Writing - original draft: M.W., A.T.; Writing - review & editing: M.W., A.G., I.M., I.G., L.B., P.W.A., I.B., K.N., M.R.G., M.P., A.T.; Supervision: I.B., M.R.G., M.P., A.T.; Project administration: A.T.; Funding acquisition: P.W.A., M.R.G., M.P., A.T.

References
Alessandri-Haber, N., Paillart, C., Arsac, C., Gola, M., Couraud, F. and Crest, M. (1999). Specific distribution of sodium channels in axons of rat embryo spinal motoneurones. *J. Physiol.* **518**, 203-214. doi:10.1111/j.1469-7793.1999.0203r.x

Alvarez-Medina, R., Cayuso, J., Okubo, T., Takada, S. and Marti, E. (2008). Wnt canonical pathway restricts graded Shh/Gli patterning activity through the regulation of Gli3 expression. *Development* **135**, 237-247. doi:10.1242/dev.012054

Amin, S., Neijts, R., Simmini, S., van Rooijen, C., Tan, S. C., Kester, L., van Oudenaarden, A., Creyghton, M. P. and Deschamps, J. (2016). Cdx and T brachyury co-activate growth signaling in the embryonic axial progenitor niche. *Cell Rep.* **17**, 3165-3177. doi:10.1016/j.celrep.2016.11.069

Amoroso, M. W., Croft, G. F., Williams, D. J., O'Keeffe, S., Carrasco, M. A., Davis, A. R., Roybon, L., Oakley, D. H., Maniatis, T., Henderson, C. E. et al. (2013). Accelerated high-yield generation of limb-innervating motor neurons from human stem cells. *J. Neurosci.* **33**, 574-586. doi:10.1523/JNEUROSCI.0906-12.2013

Anders, S. and Huber, W. (2010). Differential expression analysis for sequence count data. *Genome Biol.* **11**, R106. doi:10.1186/gb-2010-11-10-r106

Anderson, M. J., Magidson, V., Kageyama, R. and Lewandoski, M. (2020). Fgf4 maintains Hes7 levels critical for normal somite segmentation clock function. *Elife* **9**, e55608. doi:10.7554/eLife.55608

Ansari, M., Rainger, J. K., Murray, J. E., Hanson, I., Firth, H. V., Mehendale, F., Amiel, J., Gordon, C. T., Percesepe, A., Mazzanti, L. et al. (2014). A syndromic form of Pierre Robin sequence is caused by 5q23 deletions encompassing FBN2 and PHAX. *Eur. J. Med. Genet.* **57**, 587-595. doi:10.1016/j.ejmg.2014.08.007

Arber, S., Han, B., Mendelsohn, M., Smith, M., Jessell, T. M. and Sockanathan, S. (1999). Requirement for the homeobox gene Hb9 in the consolidation of motor neuron identity. *Neuron* **23**, 659-674. doi:10.1016/S0896-6273(01)80026-X

Asli, N. S. and Kessel, M. (2010). Spatiotemporally restricted regulation of generic motor neuron programs by miR-196-mediated repression of Hoxb8. *Dev. Biol.* **344**, 857-868. doi:10.1016/j.ydbio.2010.06.003

Bertero, A., Pawlowski, M., Ortmann, D., Snijders, K., Yiangou, L., Cardoso de Brito, M., Brown, S., Bernard, W. G., Cooper, J. D., Giacomelli, E. et al. (2016). Optimized inducible shRNA and CRISPR/Cas9 platforms for in vitro studies of human development using hPSCs. *Development* **143**, 4405-4418. doi:10.1242/dev.138081

Bock, C., Kiskinis, E., Verstappen, G., Gu, H., Boulting, G., Smith, Z. D., Ziller, M., Croft, G. F., Amoroso, M. W., Oakley, D. H. et al. (2011). Reference maps of human ES and iPS cell variation enable high-throughput characterization of pluripotent cell lines. *Cell* **144**, 439-452. doi:10.1016/j.cell.2010.12.032

Bosse, A., Zülch, A., Becker, M.-B., Torres, M., Gómez-Skarmeta, J. L., Modolell, J. and Gruss, P. (1997). Identification of the vertebrate Iroquois homeobox gene family with overlapping expression during early development of the nervous system. *Mech. Dev.* **69**, 169-181. doi:10.1016/S0925-4773(97)00165-2

DEVELOPMENT

Boulet, A. M. and Capecchi, M. R. (2012). Signaling by FGF4 and FGF8 is required for axial elongation of the mouse embryo. *Dev. Biol.* **371**, 235-245. doi:10.1016/j.ydbio.2012.08.017

Briscoe, J., Pierani, A., Jessell, T. M. and Ericson, J. (2000). A homeodomain protein code specifies progenitor cell identity and neuronal fate in the ventral neural tube. *Cell* **101**, 435-445. doi:10.1016/S0092-8674(00)80853-3

Brockington, A., Ning, K., Heath, P. R., Wood, E., Kirby, J., Fusi, N., Lawrence, N., Wharton, S. B., Ince, P. G. and Shaw, P. J. (2013). Unravelling the enigma of selective vulnerability in neurodegeneration: motor neurons resistant to degeneration in ALS show distinct gene expression characteristics and decreased susceptibility to excitotoxicity. *Acta Neuropathol.* **125**, 95-109. doi:10.1007/s00401-012-1058-5

Cambray, N. and Wilson, V. (2007). Two distinct sources for a population of maturing axial progenitors. *Development* **134**, 2829-2840. doi:10.1242/dev.02877

Candia, A. F., Hu, J., Crosby, J., Lalley, P. A., Noden, D., Nadeau, J. H. and Wright, C. V. (1992). Mox-1 and Mox-2 define a novel homeobox gene subfamily and are differentially expressed during early mesodermal patterning in mouse embryos. *Development* **116**, 1123-1136.

Carpenter, A. E., Jones, T. R., Lamprecht, M. R., Clarke, C., Kang, I. H., Friman, O., Guertin, D. A., Chang, J. H., Lindquist, R. A., Moffat, J. et al. (2006). CellProfiler: image analysis software for identifying and quantifying cell phenotypes. *Genome Biol.* **7**, R100. doi:10.1186/gb-2006-7-10-r100

Chambers, S. M., Fasano, C. A., Papapetrou, E. P., Tomishima, M., Sadelain, M. and Studer, L. (2009). Highly efficient neural conversion of human ES and iPS cells by dual inhibition of SMAD signaling. *Nat. Biotechnol.* **27**, 275-280. doi:10.1038/nbt.1529

Chen, J., Bardes, E. E., Aronow, B. J. and Jegga, A. G. (2009). ToppGene suite for gene list enrichment analysis and candidate gene prioritization. *Nucleic Acids Res.* **37**, W305-W311. doi:10.1093/nar/gkp427

Cooper, F., Gentsch, G. E., Mitter, E., Bouissou, C., Healy, L., Hernandez-Rodriguez, A., Smith, J. C. and Bernardo, A. S. (2020). Rostrocaudal patterning and neural crest differentiation of human pre-neural spinal cord progenitors in vitro. *bioRxiv*.

Cunningham, T. J., Kumar, S., Yamaguchi, T. P. and Duester, G. (2015). Wnt8a and Wnt3a cooperate in the axial stem cell niche to promote mammalian body axis extension. *Dev. Dyn.* **244**, 797-807. doi:10.1002/dvdy.24275

Dasen, J. S., Liu, J.-P. and Jessell, T. M. (2003). Motor neuron columnar fate imposed by sequential phases of Hox-c activity. *Nature* **425**, 926-933. doi:10.1038/nature02051

Dasen, J. S., Tice, B. C., Brenner-Morton, S. and Jessell, T. M. (2005). A Hox regulatory network establishes motor neuron pool identity and target-muscle connectivity. *Cell* **123**, 477-491. doi:10.1016/j.cell.2005.09.009

Dasen, J. S., De Camilli, A., Wang, B., Tucker, P. W. and Jessell, T. M. (2008). Hox repertoires for motor neuron diversity and connectivity gated by a single accessory factor, FoxP1. *Cell* **134**, 304-316. doi:10.1016/j.cell.2008.06.019

Davis-Dusenbery, B. N., Williams, L. A., Klim, J. R. and Eggan, K. (2014). How to make spinal motor neurons. *Development* **141**, 491-501. doi:10.1242/dev.097410

Delfino-Machin, M., Lunn, J. S., Breitkreuz, D. N., Akai, J. and Storey, K. G. (2005). Specification and maintenance of the spinal cord stem zone. *Development* **132**, 4273-4283. doi:10.1242/dev.02009

Denham, M., Hasegawa, K., Menheniott, T., Rollo, B., Zhang, D., Hough, S., Alshawaf, A., Febbraro, F., Ighaniyan, S., Leung, J. et al. (2015). Multipotent caudal neural progenitors derived from human pluripotent stem cells that give rise to lineages of the central and peripheral nervous system. *Stem Cells* **33**, 1759-1770. doi:10.1002/stem.1991

Deschamps, J. and Duboule, D. (2017). Embryonic timing, axial stem cells, chromatin dynamics, and the Hox clock. *Genes Dev.* **31**, 1406-1416. doi:10.1101/gad.303123.117

Deschamps, J. and van Nes, J. (2005). Developmental regulation of the Hox genes during axial morphogenesis in the mouse. *Development* **132**, 2931-2942. doi:10.1242/dev.01897

Desmarais, J. A., Unger, C., Damjanov, I., Meuth, M. and Andrews, P. (2016). Apoptosis and failure of checkpoint kinase 1 activation in human induced pluripotent stem cells under replication stress. *Stem Cell Res. Ther.* **7**, 17. doi:10.1186/s13287-016-0279-2

Dias, J. M., Alekseenko, Z., Applequist, J. M. and Ericson, J. (2014). Tgfβ signaling regulates temporal neurogenesis and potency of neural stem cells in the CNS. *Neuron* **84**, 927-939. doi:10.1016/j.neuron.2014.10.033

Diaz-Cuadros, M., Wagner, D. E., Budjan, C., Hubaud, A., Tarazona, O. A., Donelly, S., Michaut, A., Al Tanoury, Z., Yoshioka-Kobayashi, K., Niino, Y. et al. (2020). In vitro characterization of the human segmentation clock. *Nature* **580**, 113-118. doi:10.1038/s41586-019-1885-9

Diez del Corral, R., Breitkreuz, D. N. and Storey, K. G. (2002). Onset of neuronal differentiation is regulated by paraxial mesoderm and requires attenuation of FGF signalling. *Development* **129**, 1681-1691.

Diez del Corral, R., Olivera-Martinez, I., Goriely, A., Gale, E., Maden, M. and Storey, K. (2003). Opposing FGF and retinoid pathways control ventral neural pattern, neuronal differentiation, and segmentation during body axis extension. *Neuron* **40**, 65-79. doi:10.1016/S0896-6273(03)00565-8

Dobin, A., Davis, C. A., Schlesinger, F., Drenkow, J., Zaleski, C., Jha, S., Batut, P., Chaisson, M. and Gingeras, T. R. (2013). STAR: ultrafast universal RNA-seq aligner. *Bioinformatics* **29**, 15-21. doi:10.1093/bioinformatics/bts635

Du, Z.-W., Chen, H., Liu, H., Lu, J., Qian, K., Huang, C.-L., Zhong, X., Fan, F. and Zhang, S.-C. (2015). Generation and expansion of highly pure motor neuron progenitors from human pluripotent stem cells. *Nat. Commun.* **6**, 6626. doi:10.1038/ncomms7626

Edri, S., Hayward, P., Baillie-Johnson, P., Steventon, B. J. and Martinez Arias, A. (2019). An epiblast stem cell-derived multipotent progenitor population for axial extension. *Development* **146**, dev168187. doi:10.1242/dev.168187

Ericson, J., Thor, S., Edlund, T., Jessell, T. M. and Yamada, T. (1992). Early stages of motor neuron differentiation revealed by expression of homeobox gene Islet-1. *Science* **256**, 1555-1560. doi:10.1126/science.1350865

Estevez-Silva, M. C., Sreeram, A., Cuskey, S., Fedorchak, N., Iyer, N. and Ashton, R. S. (2018). Single-injection ex ovo transplantation method for broad spinal cord engraftment of human pluripotent stem cell-derived motor neurons. *J. Neurosci. Methods* **298**, 16-23. doi:10.1016/j.jneumeth.2018.01.006

Faustino Martins, J.-M., Fischer, C., Urzi, A., Vidal, R., Kunz, S., Ruffault, P.-L., Kabuss, L., Hube, I., Gazzerro, E., Birchmeier, C. et al. (2020). Self-organizing 3D human trunk neuromuscular organoids. *Cell Stem Cell* **26**, 172-186.e6. doi:10.1016/j.stem.2019.12.007

Frith, T. J. R. and Tsakiridis, A. (2019). Efficient generation of trunk neural crest and sympathetic neurons from human pluripotent stem cells via a neuromesodermal axial progenitor intermediate. *Curr. Protoc. Stem Cell Biol.* **49**, e81. doi:10.1002/cpsc.81

Frith, T. J. R., Granata, I., Wind, M., Stout, E., Thompson, O., Neumann, K., Stavish, D., Heath, P. R., Ortmann, D., Hackland, J. O. S. et al. (2018). Human axial progenitors generate trunk neural crest cells in vitro. *eLife* **7**, e35786. doi:10.7554/eLife.35786

Garriock, R. J., Chalamalasetty, R. B., Kennedy, M. W., Canizales, L. C., Lewandoski, M. and Yamaguchi, T. P. (2015). Lineage tracing of neuromesodermal progenitors reveals novel Wnt-dependent roles in trunk progenitor cell maintenance and differentiation. *Development* **142**, 1628-1638. doi:10.1242/dev.111922

Gerardo-Nava, J., Mayorenko, I. I., Grehl, T., Steinbusch, H. W. M., Weis, J. and Brook, G. A. (2013). Differential pattern of neuroprotection in lumbar, cervical and thoracic spinal cord segments in an organotypic rat model of glutamate-induced excitotoxicity. *J. Chem. Neuroanat.* **53**, 11-17. doi:10.1016/j.jchemneu.2013.09.007

Goto, H., Kimmey, S. C., Row, R. H., Matus, D. Q. and Martin, B. L. (2017). FGF and canonical Wnt signaling cooperate to induce paraxial mesoderm from tailbud neuromesodermal progenitors through regulation of a two-step epithelial to mesenchymal transition. *Development* **144**, 1412-1424. doi:10.1242/dev.143578

Goulding, M. D., Chalepakis, G., Deutsch, U., Erselius, J. R. and Gruss, P. (1991). Pax-3, a novel murine DNA binding protein expressed during early neurogenesis. *EMBO J.* **10**, 1135-1147. doi:10.1002/j.1460-2075.1991.tb08054.x

Gouti, M., Tsakiridis, A., Wymeersch, F. J., Huang, Y., Kleinjung, J., Wilson, V. and Briscoe, J. (2014). In vitro generation of neuromesodermal progenitors reveals distinct roles for wnt signalling in the specification of spinal cord and paraxial mesoderm identity. *PLoS Biol.* **12**, e1001937. doi:10.1371/journal.pbio.1001937

Gouti, M., Delile, J., Stamataki, D., Wymeersch, F. J., Huang, Y., Kleinjung, J., Wilson, V. and Briscoe, J. (2017). A gene regulatory network balances neural and mesoderm specification during vertebrate trunk development. *Dev. Cell* **41**, 243-261.e7. doi:10.1016/j.devcel.2017.04.002

Guillot, C., Michaut, A., Rabe, B. and Pourquié, O. (2020). Dynamics of primitive streak regression controls the fate of neuro-mesodermal progenitors in the chicken embryo. *bioRxiv*.

Hackland, J. O. S., Shelar, P. B., Sandhu, N., Prasad, M. S., Charney, R. M., Gomez, G. A., Frith, T. J. R. and García-Castro, M. I. (2019). FGF modulates the axial identity of trunk hPSC-derived neural crest but not the cranial-trunk decision. *Stem Cell Rep.* **12**, 920-933. doi:10.1016/j.stemcr.2019.04.015

Hamburger, V. and Hamilton, H. L. (1951). A series of normal stages in the development of the chick embryo. *J. Morphol.* **88**, 49-92. doi:10.1002/jmor.1050880104

Henrique, D., Abranches, E., Verrier, L. and Storey, K. G. (2015). Neuromesodermal progenitors and the making of the spinal cord. *Development* **142**, 2864-2875. doi:10.1242/dev.119768

International Stem Cell Initiative. (2018). Assessment of established techniques to determine developmental and malignant potential of human pluripotent stem cells. *Nat. Commun.* **9**, 1925. doi:10.1038/s41467-018-04011-3

Iwai, H., Shimada, H., Nishimura, S., Kobayashi, Y., Itakura, G., Hori, K., Hikishima, K., Ebise, H., Negishi, N., Shibata, S. et al. (2015). Allogeneic neural stem/progenitor cells derived from embryonic stem cells promote functional recovery after transplantation into injured spinal cord of nonhuman primates. *Stem Cells Transl. Med.* **4**, 708-719. doi:10.5966/sctm.2014-0215

Jung, H., Lacombe, J., Mazzoni, E. O., Liem, K. F., Jr., Grinstein, J., Mahony, S., Mukhopadhyay, D., Gifford, D. K., Young, R. A., Anderson, K. V. et al. (2010). Global control of motor neuron topography mediated by the repressive actions of a single hox gene. *Neuron* **67**, 781-796. doi:10.1016/j.neuron.2010.08.008

Jurberg, A. D., Aires, R., Novoa, A., Rowland, J. E. and Mallo, M. (2014). Compartment-dependent activities of Wnt3a/β-catenin signaling during vertebrate axial extension. *Dev. Biol.* **394**, 253-263. doi:10.1016/j.ydbio.2014.08.012

Kadoya, K., Lu, P., Nguyen, K., Lee-Kubli, C., Kumamaru, H., Yao, L., Knackert, J., Poplawski, G., Dulin, J. N., Strobl, H. et al. (2016). Spinal cord reconstitution with homologous neural grafts enables robust corticospinal regeneration. *Nat. Med.* **22**, 479-487. doi:10.1038/nm.4066

Kaplan, A., Spiller, K. J., Towne, C., Kanning, K. C., Choe, G. T., Geber, A., Akay, T., Aebischer, P. and Henderson, C. E. (2014). Neuronal matrix metalloproteinase-9 is a determinant of selective neurodegeneration. *Neuron* **81**, 333-348. doi:10.1016/j.neuron.2013.12.009

Kee, Y. and Bronner-Fraser, M. (2001). Id4 expression and its relationship to other Id genes during avian embryonic development. *Mech. Dev.* **109**, 341-345. doi:10.1016/S0925-4773(01)00576-7

Kondo, T., Funayama, M., Tsukita, K., Hotta, A., Yasuda, A., Nori, S., Kaneko, S., Nakamura, M., Takahashi, R., Okano, H. et al. (2014). Focal transplantation of human iPSC-derived glial-rich neural progenitors improves lifespan of ALS mice. *Stem Cell Rep.* **3**, 242-249. doi:10.1016/j.stemcr.2014.05.017

Koyanagi-Aoi, M., Ohnuki, M., Takahashi, K., Okita, K., Noma, H., Sawamura, Y., Teramoto, I., Narita, M., Sato, Y., Ichisaka, T. et al. (2013). Differentiation-defective phenotypes revealed by large-scale analyses of human pluripotent stem cells. *Proc. Natl. Acad. Sci. USA* **110**, 20569-20574. doi:10.1073/pnas.1319061110

Kumamaru, H., Kadoya, K., Adler, A. F., Takashima, Y., Graham, L., Coppola, G. and Tuszynski, M. H. (2018). Generation and post-injury integration of human spinal cord neural stem cells. *Nat. Methods* **15**, 723-731. doi:10.1038/s41592-018-0074-3

Lacombe, J., Hanley, O., Jung, H., Philippidou, P., Surmeli, G., Grinstein, J. and Dasen, J. S. (2013). Genetic and functional modularity of Hox activities in the specification of limb-innervating motor neurons. *PLoS Genet.* **9**, e1003184. doi:10.1371/journal.pgen.1003184

Lee, K. J., Mendelsohn, M. and Jessell, T. M. (1998). Neuronal patterning by BMPs: a requirement for GDF7 in the generation of a discrete class of commissural interneurons in the mouse spinal cord. *Genes Dev.* **12**, 3394-3407. doi:10.1101/gad.12.21.3394

Li, B. and Dewey, C. N. (2011). RSEM: accurate transcript quantification from RNA-seq data with or without a reference genome. *BMC Bioinformatics* **12**, 323. doi:10.1186/1471-2105-12-323

Libby, A. R. G., Joy, D. A., Elder, N. H., Bulger, E. A., Krakora, M. Z., Gaylord, E. A., Mendoza-Camacho, F. and McDevitt, T. C. (2020). Axial elongation of caudalized human pluripotent stem cell organoids mimics neural tube development. *bioRxiv*.

Lichtig, H., Artamonov, A., Polevoy, H., Reid, C. D., Bielas, S. L. and Frank, D. (2020). Modeling bainbridge-ropers syndrome in Xenopus laevis Embryos. *Front. Physiol.* **11**, 75. doi:10.3389/fphys.2020.00075

Lieberam, I., Agalliu, D., Nagasawa, T., Ericson, J. and Jessell, T. M. (2005). A Cxcl12-CXCR4 chemokine signaling pathway defines the initial trajectory of mammalian motor axons. *Neuron* **47**, 667-679. doi:10.1016/j.neuron.2005.08.011

Liem, K. F., Jr., Jessell, T. M. and Briscoe, J. (2000). Regulation of the neural patterning activity of sonic hedgehog by secreted BMP inhibitors expressed by notochord and somites. *Development* **127**, 4855-4866.

Lippmann, E. S., Williams, C. E., Ruhl, D. A., Estevez-Silva, M. C., Chapman, E. R., Coon, J. J. and Ashton, R. S. (2015). Deterministic HOX patterning in human pluripotent stem cell-derived neuroectoderm. *Stem Cell Rep.* **4**, 632-644. doi:10.1016/j.stemcr.2015.02.018

Lopez-Yrigoyen, M., Fidanza, A., Cassetta, L., Axton, R. A., Taylor, A. H., Meseguer-Ripolles, J., Tsakiridis, A., Wilson, V., Hay, D. C., Pollard, J. W. et al. (2018). A human iPSC line capable of differentiating into functional macrophages expressing ZsGreen: a tool for the study and in vivo tracking of therapeutic cells. *Philos. Trans. R. Soc. Biol. Sci.* **373**, 20170219. doi:10.1098/rstb.2017.0219

Love, M. I., Huber, W. and Anders, S. (2014). Moderated estimation of fold change and dispersion for RNA-seq data with DESeq2. *Genome Biol.* **15**, 550. doi:10.1186/s13059-014-0550-8

Lu, Q. R., Sun, T., Zhu, Z., Ma, N., Garcia, M., Stiles, C. D. and Rowitch, D. H. (2002). Common developmental requirement for Olig function indicates a motor neuron/oligodendrocyte connection. *Cell* **109**, 75-86. doi:10.1016/S0092-8674(02)00678-5

Lu, P., Woodruff, G., Wang, Y., Graham, L., Hunt, M., Wu, D., Boehle, E., Ahmad, R., Poplawski, G., Brock, J. et al. (2014). Long-distance axonal growth from human induced pluripotent stem cells after spinal cord injury. *Neuron* **83**, 789-796. doi:10.1016/j.neuron.2014.07.014

Lu, P., Ceto, S., Wang, Y., Graham, L., Wu, D., Kumamaru, H., Staufenberg, E. and Tuszynski, M. H. (2017). Prolonged human neural stem cell maturation supports recovery in injured rodent CNS. *J. Clin. Invest.* **127**, 3287-3299. doi:10.1172/JCI92955

Lumb, R., Buckberry, S., Secker, G., Lawrence, D. and Schwarz, Q. (2017). Transcriptome profiling reveals expression signatures of cranial neural crest cells arising from different axial levels. *BMC Dev. Biol.* **17**, 5. doi:10.1186/s12861-017-0147-z

Ma, T. C., Vong, K. I. and Kwan, K. M. (2020). Spatiotemporal decline of BMP signaling activity in neural progenitors mediates fate transition and safeguards neurogenesis. *Cell Rep.* **30**, 3616-3624.e4. doi:10.1016/j.celrep.2020.02.089

Mathis, L., Kulesa, P. M. and Fraser, S. E. (2001). FGF receptor signalling is required to maintain neural progenitors during Hensen's node progression. *Nat. Cell Biol.* **3**, 559-566. doi:10.1038/35078535

Maury, Y., Côme, J., Piskorowski, R. A., Salah-Mohellibi, N., Chevaleyre, V., Peschanski, M., Martinat, C. and Nedelec, S. (2015). Combinatorial analysis of developmental cues efficiently converts human pluripotent stem cells into multiple neuronal subtypes. *Nat. Biotechnol.* **33**, 89-96. doi:10.1038/nbt.3049

McMahon, J. A., Takada, S., Zimmerman, L. B., Fan, C.-M., Harland, R. M. and McMahon, A. P. (1998). Noggin-mediated antagonism of BMP signaling is required for growth and patterning of the neural tube and somite. *Genes Dev.* **12**, 1438-1452. doi:10.1101/gad.12.10.1438

Mendelsohn, A. I., Dasen, J. S. and Jessell, T. M. (2017). Divergent Hox coding and evasion of retinoid signaling specifies motor neurons innervating digit muscles. *Neuron* **93**, 792-805.e4. doi:10.1016/j.neuron.2017.01.017

Metzis, V., Steinhauser, S., Pakanavicius, E., Gouti, M., Stamataki, D., Ivanovitch, K., Watson, T., Rayon, T., Mousavy Gharavy, S. N., Lovell-Badge, R. et al. (2018). Nervous system regionalization entails axial allocation before neural differentiation. *Cell* **175**, 1105-1118.e17. doi:10.1016/j.cell.2018.09.040

Mouilleau, V., Vaslin, C., Gribaudo, S., Robert, R., Nicolas, N., Jarrige, M., Terray, A., Lesueur, L., Mathis, M. W., Croft, G. et al. (2020). Dynamic extrinsic pacing of the HOX clock in human axial progenitors controls motor neuron subtype specification. *bioRxiv*.

Mugele, D., Moulding, D. A., Savery, D., Mole, M. A., Greene, N. D. A., Martinez-Barbera, J. P. and Copp, A. J. (2018). Genetic approaches in mice demonstrate that neuro-mesodermal progenitors express T/Brachyury but not Sox2. *bioRxiv*.

Muroyama, Y., Fujihara, M., Ikeya, M., Kondoh, H. and Takada, S. (2002). Wnt signaling plays an essential role in neuronal specification of the dorsal spinal cord. *Genes Dev.* **16**, 548-553. doi:10.1101/gad.937102

Nichterwitz, S., Chen, G., Aguila Benitez, J., Yilmaz, M., Storvall, H., Cao, M., Sandberg, R., Deng, Q. and Hedlund, E. (2016). Laser capture microscopy coupled with Smart-seq2 for precise spatial transcriptomic profiling. *Nat. Commun.* **7**, 12139. doi:10.1038/ncomms12139

Nijssen, J., Comley, L. H. and Hedlund, E. (2017). Motor neuron vulnerability and resistance in amyotrophic lateral sclerosis. *Acta Neuropathol.* **133**, 863-885. doi:10.1007/s00401-017-1708-8

Nishizawa, M., Chonabayashi, K., Nomura, M., Tanaka, A., Nakamura, M., Inagaki, A., Nishikawa, M., Takei, I., Oishi, A., Tanabe, K. et al. (2016). Epigenetic variation between human induced pluripotent stem cell lines is an indicator of differentiation capacity. *Cell Stem Cell* **19**, 341-354. doi:10.1016/j.stem.2016.06.019

Nordström, U., Maier, E., Jessell, T. M. and Edlund, T. (2006). An early role for WNT signaling in specifying neural patterns of Cdx and Hox gene expression and motor neuron subtype identity. *PLoS Biol.* **4**, e252. doi:10.1371/journal.pbio.0040252

Novitch, B. G., Chen, A. I. and Jessell, T. M. (2001). Coordinate regulation of motor neuron subtype identity and pan-neuronal properties by the bHLH repressor Olig2. *Neuron* **31**, 773-789. doi:10.1016/S0896-6273(01)00407-X

Olivera-Martinez, I. and Storey, K. G. (2007). Wnt signals provide a timing mechanism for the FGF-retinoid differentiation switch during vertebrate body axis extension. *Development* **134**, 2125-2135. doi:10.1242/dev.000216

Olivera-Martinez, I., Harada, H., Halley, P. A. and Storey, K. G. (2012). Loss of FGF-dependent mesoderm identity and rise of endogenous retinoid signalling determine cessation of body axis elongation. *PLoS Biol.* **10**, e1001415. doi:10.1371/journal.pbio.1001415

Olivera-Martinez, I., Schurch, N., Li, R. A., Song, J., Halley, P. A., Das, R. M., Burt, D. W., Barton, G. J. and Storey, K. G. (2014). Major transcriptome re-organisation and abrupt changes in signalling, cell cycle and chromatin regulation at neural differentiation in vivo. *Development* **141**, 3266-3276. doi:10.1242/dev.112623

Osorno, R., Tsakiridis, A., Wong, F., Cambray, N., Economou, C., Wilkie, R., Blin, G., Scotting, P. J., Chambers, I. and Wilson, V. (2012). The developmental dismantling of pluripotency is reversed by ectopic Oct4 expression. *Development* **139**, 2288-2298. doi:10.1242/dev.078071

Peljto, M., Dasen, J. S., Mazzoni, E. O., Jessell, T. M. and Wichterle, H. (2010). Functional diversity of ESC-derived motor neuron subtypes revealed through intraspinal transplantation. *Cell Stem Cell* **7**, 355-366. doi:10.1016/j.stem.2010.07.013

Philippidou, P. and Dasen, J. S. (2013). Hox genes: choreographers in neural development, architects of circuit organization. *Neuron* **80**, 12-34. doi:10.1016/j.neuron.2013.09.020

Placzek, M. and Briscoe, J. (2018). Sonic hedgehog in vertebrate neural tube development. *Int. J. Dev. Biol.* **62**, 225-234. doi:10.1387/ijdb.170293jb

Rada-Iglesias, A., Bajpai, R., Prescott, S., Brugmann, S. A., Swigut, T. and Wysocka, J. (2012). Epigenomic annotation of enhancers predicts transcriptional regulators of human neural crest. *Cell Stem Cell* **11**, 633-648. doi:10.1016/j.stem.2012.07.006

Rayon, T., Stamataki, D., Perez-Carrasco, R., Garcia-Perez, L., Barrington, C., Melchionda, M., Exelby, K., Lazaro, J., Tybulewicz, V. L. J., Fisher, E. M. C. et al. (2020). Species-specific pace of development is associated with differences in protein stability. *Science* **369**, eaba7667. doi:10.1126/science.aba7667

Sabourin, J.-C., Ackema, K. B., Ohayon, D., Guichet, P.-O., Perrin, F. E., Garces, A., Ripoll, C., Charité, J., Simonneau, L., Kettenmann, H. et al. (2009). A mesenchymal-like ZEB1⁺ niche harbors dorsal radial glial fibrillary acidic protein-positive stem cells in the spinal cord. *Stem Cells* **27**, 2722-2733. doi:10.1002/stem.226

Sagner, A. and Briscoe, J. (2019). Establishing neuronal diversity in the spinal cord: a time and a place. *Development* **146**, dev182154. doi:10.1242/dev.182154

Sagner, A., Gaber, Z. B., Delile, J., Kong, J. H., Rousso, D. L., Pearson, C. A., Weicksel, S. E., Melchionda, M., Mousavy Gharavy, S. N., Briscoe, J. et al. (2018). Olig2 and Hes regulatory dynamics during motor neuron differentiation revealed by single cell transcriptomics. *PLoS Biol.* **16**, e2003127. doi:10.1371/journal.pbio.2003127

Sagner, A., Zhang, I., Watson, T., Lazaro, J., Melchionda, M. and Briscoe, J. (2020). Temporal patterning of the central nervous system by a shared transcription factor code. *BioRxiv*.

Sander, M., Paydar, S., Ericson, J., Briscoe, J., Berber, E., German, M., Jessell, T. M. and Rubenstein, J. L. R. (2000). Ventral neural patterning by Nkx homeobox genes: Nkx6.1 controls somatic motor neuron and ventral interneuron fates. *Genes Dev.* **14**, 2134-2139. doi:10.1101/gad.820400

Shimada, K., Tachibana, T., Fujimoto, K., Sasaki, T. and Okabe, M. (2012). Temporal and spatial cellular distribution of neural crest derivatives and alpha cells during islet development. *Acta Histochem. Cytochem.* **45**, 65-75. doi:10.1267/ahc.11052

Sommer, L., Ma, Q. and Anderson, D. J. (1996). neurogenins, a novel family ofatonal-related bHLH transcription factors, are putative mammalian neuronal determination genes that reveal progenitor cell heterogeneity in the developing CNS and PNS. *Mol. Cell Neurosci.* **8**, 221-241. doi:10.1006/mcne.1996.0060

Soundararajan, P., Miles, G. B., Rubin, L. L., Brownstone, R. M. and Rafuse, V. F. (2006). Motoneurons derived from embryonic stem cells express transcription factors and develop phenotypes characteristic of medial motor column neurons. *J. Neurosci.* **26**, 3256-3268. doi:10.1523/JNEUROSCI.5537-05.2006

Storey, K. G., Goriely, A., Sargent, C. M., Brown, J. M., Burns, H. D., Abud, H. M. and Heath, J. K. (1998). Early posterior neural tissue is induced by FGF in the chick embryo. *Development* **125**, 473-484.

Takada, S., Stark, K. L., Shea, M. J., Vassileva, G., McMahon, J. A. and McMahon, A. P. (1994). Wnt-3a regulates somite and tailbud formation in the mouse embryo. *Genes Dev.* **8**, 174-189. doi:10.1101/gad.8.2.174

Takebayashi, H., Nabeshima, Y., Yoshida, S., Chisaka, O., Ikenaka, K. and Nabeshima, Y.-I. (2002). The basic helix-loop-helix factor olig2 is essential for the development of motoneuron and oligodendrocyte lineages. *Curr. Biol.* **12**, 1157-1163. doi:10.1016/S0960-9822(02)00926-0

Takemoto, T., Uchikawa, M., Kamachi, Y. and Kondoh, H. (2006). Convergence of Wnt and FGF signals in the genesis of posterior neural plate through activation of the Sox2 enhancer N-1. *Development* **133**, 297-306. doi:10.1242/dev.02196

Takemoto, T., Uchikawa, M., Yoshida, M., Bell, D. M., Lovell-Badge, R., Papaioannou, V. E. and Kondoh, H. (2011). Tbx6-dependent Sox2 regulation determines neural or mesodermal fate in axial stem cells. *Nature* **470**, 394-398. doi:10.1038/nature09729

Thaler, J., Harrison, K., Sharma, K., Lettieri, K., Kehrl, J. and Pfaff, S. L. (1999). Active suppression of interneuron programs within developing motor neurons revealed by analysis of homeodomain factor HB9. *Neuron* **23**, 675-687. doi:10.1016/S0896-6273(01)80027-1

Thaler, J. P., Koo, S. J., Kania, A., Lettieri, K., Andrews, S., Cox, C., Jessell, T. M. and Pfaff, S. L. (2004). A postmitotic role for Isl-class LIM homeodomain proteins in the assignment of visceral spinal motor neuron identity. *Neuron* **41**, 337-350. doi:10.1016/S0896-6273(04)00011-X

Thomson, J. A., Itskovitz-Eldor, J., Shapiro, S. S., Waknitz, M. A., Swiergiel, J. J., Marshall, V. S. and Jones, J. M. (1998). Embryonic stem cell lines derived from human blastocysts. *Science* **282**, 1145-1147. doi:10.1126/science.282.5391.1145

Timmer, J. R., Wang, C. and Niswander, L. (2002). BMP signaling patterns the dorsal and intermediate neural tube via regulation of homeobox and helix-loop-helix transcription factors. *Development* **129**, 2459-2472.

Tsakiridis, A. and Wilson, V. (2015). Assessing the bipotency of in vitro-derived neuromesodermal progenitors. *F1000Res* **4**, 100. doi:10.12688/f1000research.6345.1

Tsakiridis, A., Huang, Y., Blin, G., Skylaki, S., Wymeersch, F., Osorno, R., Economou, C., Karagianni, E., Zhao, S., Lowell, S. et al. (2014). Distinct Wnt-driven primitive streak-like populations reflect in vivo lineage precursors. *Development* **141**, 1209-1221. doi:10.1242/dev.101014

Tsuchida, T., Ensini, M., Morton, S. B., Baldassare, M., Edlund, T., Jessell, T. M. and Pfaff, S. L. (1994). Topographic organization of embryonic motor neurons defined by expression of LIM homeobox genes. *Cell* **79**, 957-970. doi:10.1016/0092-8674(94)90027-2

Tsuji, O., Miura, K., Okada, Y., Fujiyoshi, K., Mukaino, M., Nagoshi, N., Kitamura, K., Kumagai, G., Nishino, M., Tomisato, S. et al. (2010). Therapeutic potential of appropriately evaluated safe-induced pluripotent stem cells for spinal cord injury. *Proc. Natl. Acad. Sci. USA* **107**, 12704-12709. doi:10.1073/pnas.0910106107

Turner, D. A., Hayward, P. C., Baillie-Johnson, P., Rue, P., Broome, R., Faunes, F. and Martinez Arias, A. (2014). Wnt/beta-catenin and FGF signalling direct the specification and maintenance of a neuromesodermal axial progenitor in ensembles of mouse embryonic stem cells. *Development* **141**, 4243-4253. doi:10.1242/dev.112979

Tzouanacou, E., Wegener, A., Wymeersch, F. J., Wilson, V. and Nicolas, J.-F. (2009). Redefining the progression of lineage segregations during mammalian embryogenesis by clonal analysis. *Dev. Cell* **17**, 365-376. doi:10.1016/j.devcel.2009.08.002

Vallstedt, A., Muhr, J., Pattyn, A., Pierani, A., Mendelsohn, M., Sander, M., Jessell, T. M. and Ericson, J. (2001). Different levels of repressor activity assign redundant and specific roles to Nkx6 genes in motor neuron and interneuron specification. *Neuron* **31**, 743-755. doi:10.1016/S0896-6273(01)00412-3

van den Akker, E., Forlani, S., Chawengsaksophak, K., de Graaff, W., Beck, F., Meyer, B. I. and Deschamps, J. (2002). Cdx1 and Cdx2 have overlapping functions in anteroposterior patterning and posterior axis elongation. *Development* **129**, 2181-2193.

Verrier, L., Davidson, L., Gierliński, M., Dady, A. and Storey, K. G. (2018). Neural differentiation, selection and transcriptomic profiling of human neuromesodermal progenitor-like cells in vitro. *Development* **145**, dev166215. doi:10.1242/dev.166215

Wetts, R. and Vaughn, J. E. (1994). Choline Acetyltransferase and NADPH Diaphorase are co-expressed in rat spinal cord neurons. *Neuroscience* **63**, 1117-1124. doi:10.1016/0306-4522(94)90577-0

Wichterle, H., Lieberam, I., Porter, J. A. and Jessell, T. M. (2002). Directed differentiation of embryonic stem cells into motor neurons. *Cell* **110**, 385-397. doi:10.1016/S0092-8674(02)00835-8

William, C. M., Tanabe, Y. and Jessell, T. M. (2003). Regulation of motor neuron subtype identity by repressor activity of Mnx class homeodomain proteins. *Development* **130**, 1523-1536. doi:10.1242/dev.00358

Wood, H. B. and Episkopou, V. (1999). Comparative expression of the mouse Sox1, Sox2 and Sox3 genes from pre-gastrulation to early somite stages. *Mech. Dev.* **86**, 197-201. doi:10.1016/S0925-4773(99)00116-1

Wood, T. R., Kyrsting, A., Stegmaier, J., Kucinski, I., Kaminski, C. F., Mikut, R. and Voiculescu, O. (2019). Neuromesodermal progenitors separate the axial stem zones while producing few single- and dual-fated descendants. *bioRiv*.

Wymeersch, F. J., Huang, Y., Blin, G., Cambray, N., Wilkie, R., Wong, F. C. K. and Wilson, V. (2016). Position-dependent plasticity of distinct progenitor types in the primitive streak. *eLife* **5**, e10042. doi:10.7554/eLife.10042

Wymeersch, F. J., Skylaki, S., Huang, Y., Watson, J. A., Economou, C., Marek-Johnston, C., Tomlinson, S. R. and Wilson, V. (2019). Transcriptionally dynamic progenitor populations organised around a stable niche drive axial patterning. *Development* **146**, dev168161. doi:10.1242/dev.168161

Yohn, D. C., Miles, G. B., Rafuse, V. F. and Brownstone, R. M. (2008). Transplanted mouse embryonic stem-cell-derived motoneurons form functional motor units and reduce muscle atrophy. *J. Neurosci.* **28**, 12409-12418. doi:10.1523/JNEUROSCI.1761-08.2008

Young, T., Rowland, J. E., van de Ven, C., Bialecka, M., Novoa, A., Carapuco, M., van Nes, J., de Graaff, W., Duluc, I., Freund, J.-N. et al. (2009). Cdx and Hox genes differentially regulate posterior axial growth in mammalian embryos. *Dev. Cell* **17**, 516-526. doi:10.1016/j.devcel.2009.08.010

Zalfa, C., Rota Nodari, L., Vacchi, E., Gelati, M., Profico, D., Boido, M., Binda, E., De Filippis, L., Copetti, M., Garlatti, V. et al. (2019). Transplantation of clinical-grade human neural stem cells reduces neuroinflammation, prolongs survival and delays disease progression in the SOD1 rats. *Cell Death Dis.* **10**, 345. doi:10.1038/s41419-019-1582-5

Zeisel, A., Hochgerner, H., Lönnerberg, P., Johnsson, A., Memic, F., van der Zwan, J., Häring, M., Braun, E., Borm, L. E., La Manno, G. et al. (2018). Molecular architecture of the mouse nervous system. *Cell* **174**, 999-1014.e22. doi:10.1016/j.cell.2018.06.021

Zhang, X., Huang, C. T., Chen, J., Pankratz, M. T., Xi, J., Li, J., Yang, Y., Lavaute, T. M., Li, X.-J., Ayala, M. et al. (2010). Pax6 is a human neuroectoderm cell fate determinant. *Cell Stem Cell* **7**, 90-100. doi:10.1016/j.stem.2010.04.017

DEVELOPMENT